University of Southern California

Final Design Project

AME-261: Basic Flight Mechanics

Borealis

Team 9

Justin Perlman, Cormac Herbert, Mahmoud Tohfi, Jayden Cho, Noah Walls

Department of Aerospace and Mechanical Engineering

May 7, 2026

University of Southern California

Abstract

USC Viterbi Department of Aerospace and Mechanical Engineering

Borealis

The design proposal to create a competitive Arctic Short Take-Off and Landing (STOL) aircraft requires the balance of robust engineering and superior aerodynamic principles to ensure safe and reliable operations north of the Arctic Circle. While remaining compliant with planned 14 CFR Part 23 certification, Borealis maintains exceptional versatility across three distinct mission profiles, seamlessly transitioning between a 9-passenger transport, a heavy-cargo hauler, and a critical medical evacuation platform. Borealis, designed for extreme environments, meets and exceeds the reference mission range requirement of 450 nmi, rate of climb constraints of at least 800 ft/min at maximum takeoff weight, and boasts a maximum operating velocity V_{NE} exceeding 180 KTAS.

Furthermore, Borealis features specialized landing gear and ruggedized construction to consistently operate on unprepared gravel surfaces in temperatures as low as -30°F. Incorporating the latest in avionics and Flight Into Known Icing (FIKI) certification, the flight deck provides the two-pilot crew ample resources to safely conduct any phase of flight amidst unpredictable weather and minimal supporting infrastructure. In order to design Borealis, the team carefully negotiated the boundary between a high-capacity utility aircraft and an efficient cruiser to generate a highly reliable platform with low direct operating costs, maximizing operator profitability without compromising safety. With focused attention to ease of boarding, cargo loading, and patient transport, Borealis's pragmatic yet crisp design masks the impressive performance characteristics required to thrive in one of the world's harshest climates.

Welcome to Borealis.

Table of Contents

Chapter 1
Introduction

1.1 Executive Summary

Borealis is a high-wing, twin-turboprop Short Takeoff and Landing (STOL) aircraft designed to certify under 14 CFR Part 23 for operation north of the Arctic Circle. Configured around a wing mounted twin-engine layout with a cruciform empennage and retractable tricycle landing gear, Borealis is powered by two Pratt & Whitney Canada PT6A-60A turboprops producing 772 kW each at sea level, with propeller efficiencies of 0.85 in cruise and 0.75 in climb. The airframe is reconfigurable across three mission profiles — nine-passenger transport, equivalent-weight cargo, and aerial ambulance — and is certified for flight into known icing (FIKI) with reliable cold-weather operation down to −30 °F. The wing spans 28.6 m with a mean chord of 3.5 m and 2° incidence, and the aircraft operates at a maximum takeoff weight of 58.5 kN with an empty weight fraction of 0.76. Figure 1.1 presents the layout of Borealis. Through deliberate optimization of wing geometry, high-lift devices, and powerful propulsion, Borealis delivers robust field performance on unprepared surfaces while maintaining low direct operating costs across the reference and medevac mission profiles. Of special note:

1. V_{max} greater than 180 KTAS, satisfying the RFP cruise requirement at 275.6 KTAS
2. R/C_{max} greater than 800 ft/min at MTOW under ISA+5 conditions, satisfying requirements at 3543 ft/min
3. Reference mission range exceeds 450 nmi at an average ground speed above 130 KTAS, with a demonstrated cruise capability above 833 km at 9 km altitude.
4. Takeoff and landing field length under 500 ft over a 50 ft obstacle on gravel.
5. Service ceiling above 18,000 ft with full FIKI certification, satisfying requirements at a service ceiling height of 29,500 ft
6. Competitive direct operating costs per seat-mile among comparable STOL platforms in its class, costs minimized from common commercial engines and simple design, meaning maintenance and parts are cheaper.

1.2 Background and Design Considerations

Aviation has long served as a critical lifeline for remote and isolated communities, where geographic barriers and harsh environmental conditions render conventional ground transportation impractical or impossible. Nowhere is this more evident than in the Arctic regions, where approximately four million people inhabit small, dispersed settlements scattered across vast expanses of tundra, ice, and unforgiving terrain. For these communities, aircraft are not a convenience but a necessity, providing essential transportation of passengers, cargo, and emergency medical services that connect them to the broader world.

The aviation industry has historically responded to the demands of Arctic operations with a small but distinguished class of rugged utility aircraft. Iconic platforms such as the de Havilland Canada DHC-6 Twin Otter, the Cessna 208 Caravan, and the Antonov An-26 have established the operational benchmarks for cold-weather, short-field performance. These aircraft share several defining traits: high-wing configurations for ground clearance and visibility, robust landing gear capable of handling unprepared surfaces, turboprop propulsion for reliability and high static thrust, and design philosophies that prioritize maintainability over aerodynamic refinement. The Twin Otter, in particular, has remained in production and service for over five decades, a testament to the enduring need for purpose-built Arctic aircraft. However, many of these legacy designs are aging, fuel-inefficient by modern standards, and were not originally certified for flight into known icing (FIKI) conditions, leaving a notable gap in the market for a modern successor.

Recent advances in turboprop technology, composite materials, and ice protection systems have created an opportunity to develop a new generation of Arctic STOL aircraft that can meet contemporary certification standards while improving operating economics. Engines such as the Pratt & Whitney Canada PT6A series continue to evolve, offering improved specific fuel consumption and reliability. Concurrently, advances in cabin reconfiguration systems, avionics integration, and anti-icing technologies provide designers with tools to create a single airframe capable of serving multiple mission profiles without sacrificing performance in any of them.

In order to design an aircraft that addresses these needs, the lessons learned from decades of Arctic operations were synthesized with modern design methodologies to produce a competitive offering for the 2033 entry-into-service window. The proposed aircraft must successfully balance the often-competing demands of short-field performance, range, payload flexibility, and operating cost while maintaining strict compliance with 14 CFR Part 23 certification requirements. To remain viable in the Arctic utility market, the aircraft must meet or exceed the baseline performance metrics summarized in Table 1.2.

Performance Parameter	**Imperial Units**	**SI Units**
Service Ceiling (Minimum)	18,000 [ft]	5,486 [m]
Rate of Climb at MTOW, ISA+5	800 [fpm]	4.06 [m/s]

Maximum Velocity (V_{NE})	180 [KTAS]	92.6 [m/s]
Takeoff Distance over 50 ft Obstacle	500 [ft]	152 [m]
Landing Distance over 50 ft Obstacle	500 [ft]	152 [m]
Cold Weather Operation (Minimum)	-30 [°F]	-34.4 [°C]
Reference Mission Range (Minimum)	450 [nmi]	833 [km]
Reference Mission Cruise Speed (Minimum)	130 [KTAS]	66.9 [m/s]
Medevac Mission Range (Each Leg)	350 [nmi]	648 [km]
Passenger Capacity (Configuration 1)	9 PAX + 2 Crew	9 PAX + 2 Crew
Maximum Payload	2,250 [lb]	1,021 [kg]

Table 1.2 Baseline Performance Requirements

The requirements in Table 1.2 represent the minimum performance thresholds dictated by the operational realities of Arctic service. Meeting them under the additional constraints of FIKI certification, gravel runway capability, and operation at temperatures down to -30°F demands a design approach in which every subsystem is evaluated not only for its individual performance contribution but also for its compatibility with the harsh operating environment. Furthermore, because the aircraft must be reconfigurable between passenger, cargo, and aerial ambulance roles, the cabin and structural design must accommodate rapid mission transitions without imposing weight or complexity penalties that compromise baseline performance.

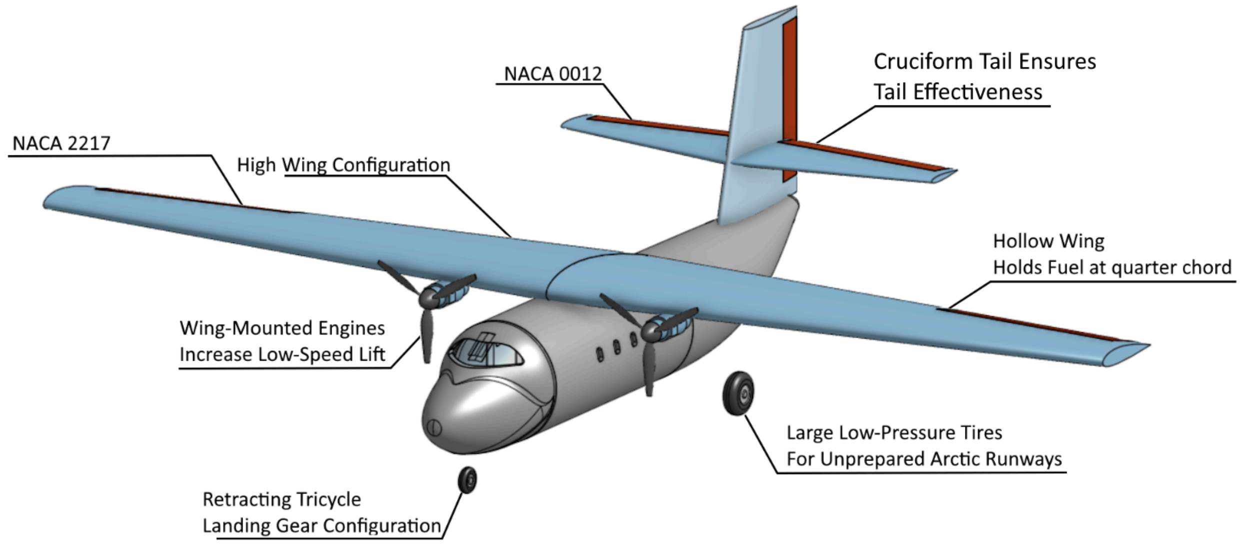

Figure 1.1: Isometric View of Borealis with labels

In conducting the design process of this aircraft, the various subsets of design work were stratified to ensure an efficient and well-coordinated workflow. To manage the technical calculations and trade studies, MATLAB modeling responsibilities were divided across the team according to discipline. Justin led wing design and airfoil characterization, including AVL simulation and lift distribution analysis. Cormac directed fuselage geometry, internal layout, and the associated drag buildup, with attention to ensuring the cross-section accommodates all three mission configurations. Mahmoud led propulsion analysis and engine downselection, evaluating candidate turboprops against the takeoff, climb, and cruise requirements. Stability and control analysis, including tail sizing and elevator effectiveness, was conducted collaboratively in the later stages of the project, with the supporting MATLAB scripts maintained on a shared Google Drive workspace to enable iterative refinement as design parameters evolved. Report generation, CAD modeling, and verification of computational results through hand calculations were distributed across the team to ensure that each major analytical result was independently checked before being incorporated into the final design.

Chapter 2

Theory

2.1 Flight Parameters

To accurately model the performance of the Borealis aircraft in intense Arctic environments, detailed atmospheric modeling was incorporated into the preliminary design phase. All flight conditions were analyzed utilizing the International Standard Atmosphere (ISA) with a +5°C temperature offset, paired with zero wind parameters, to provide a conservative baseline for all aerodynamic and propulsive estimates as mandated by the design requirements. The atmospheric density, ϱ, is the fundamental property governing aerodynamic forces and is calculated within the ISA+5 model.

To account for the variation of engine power and aerodynamic efficiency with altitude, the density ratio, σ, is defined as the local density divided by the standard sea-level density, ρ_{SL}:

$$\sigma = \frac{\rho}{\rho_{SL}}$$

The dynamic pressure, q, governs the magnitude of the aerodynamic forces experienced by the airframe and is defined by the true airspeed, V, and the local density:

$$q = \frac{1}{2}\rho V^2$$

This leads directly to the core equations for the Lift (L) and Drag (D) forces acting on the aircraft. These forces are expressed using the wing reference area (S) and their respective non-dimensional coefficients, C_L and C_D:

$$L = qSC_L \quad ; \quad D = qSC_D$$

2.2 Airfoil Selection and 3D Wing Aerodynamics

A simulation of the entire flight profile across the passenger, cargo, and medical evacuation configurations was used to evaluate the aerodynamic capabilities of the aircraft. Due to the strict landing field constraints, the design prioritized finding an optimal balance between low-speed lift required for Short Take-Off and Landing (STOL) operations and efficient high-speed cruise performance. The NACA 2217 airfoil was selected due to its inherently high maximum lift coefficient, which allows for the lower stall speeds necessary to operate on restricted Arctic runways. To verify and validate the choice of airfoil and ensure sufficient lift margins, aerodynamic modeling transitioned from 2D section data generated via XFOIL to 3D wing analysis utilizing AVL.

To satisfy the STOL requirements, the stall velocity (V_{stall}) must be minimized, as it dictates the takeoff and landing reference speeds. The stall velocity is defined by the maximum lift coefficient ($C_{L,max}$) and the instantaneous weight of the aircraft (W):

$$V_{stall} = \sqrt{\frac{2W}{\rho S C_{L,max}}}$$

Due to the decreasing density at elevated altitudes and varying environmental conditions, the required takeoff and landing velocities scale inversely with the square root of the density ratio. To drastically increase $C_{L,max}$ and lower V_{stall}, Fowler flaps are implemented in the design. Deploying these high-lift devices significantly shifts the lift curve, increasing the maximum lift coefficient to an estimated 3.21 to provide a critical safety margin during low-speed operations.

2.3 Drag Buildup and Aerodynamic Efficiency

The aerodynamic efficiency of Borealis is paramount for maintaining straight and level flight during extended missions over remote northern territories. The fundamental balance of thrust equating to drag is an essential requirement for unaccelerated flight. Consequently, drag is represented nondimensionally by the coefficient of drag, expressed as:

$$C_D = \frac{D}{qS}$$

where D represents the total drag force, q is the dynamic pressure, and S is the reference wing area.

At the relatively low speeds typical of short takeoff and landing operations, drag is predominantly composed of two aerodynamic phenomena: parasite drag, which is a function of the aircraft's wetted surface area, and induced drag, which is a byproduct of the airfoil's lift generation. To calculate the physical drag force, the coefficient equation is rewritten to express D in terms of C_D, q, and S:

$$D = C_D * q * S$$

To guarantee overall accuracy in performance models, the individual components of the drag coefficient, specifically the parasite drag coefficient ($C_{D,0}$) and the induced drag coefficient ($C_{D,i}$, must be accurately determined. The preliminary assumption remains that drag is solely a function of these two parameters at speeds below Mach 0.3; however, if the aircraft exceeds this threshold to meet its 180 KTAS maximum velocity requirement, compressible drag effects must also be incorporated.

Parasite drag is heavily influenced by the fuselage, especially given the substantial internal volume required to transport 9 passengers or large payloads like an 8,000-Watt generator and 55 gallons of diesel fuel. The parasite drag coefficient contribution strictly from the fuselage is calculated using an ellipsoid approximation:

$$C_{D,o,fuse} = [1 + 1.5(\frac{l}{d})^{-1.5} + 7(\frac{l}{d})^{-3}] * C_f$$

where l is the length of the representative ellipsoid, d is its maximum diameter, and C_f is the coefficient of friction determined via flat plate formulas utilizing the Reynolds number over the fuselage length. With this coefficient established, the physical drag force of the fuselage is given by:

$$D_{fuse} = C_{D,o,fuse} S_{wet} q_\infty = [1 + 1.5(\frac{l}{d})^{-1.5} + 7(\frac{l}{d})^{-3}] * C_f S_{wet} q_\infty$$

The wetted area, S_{wet}, is approximated by:

$$S_{wet} = \frac{\pi d}{2}(d + l)$$

and the corresponding volume of this prolate ellipsoid, representing the fuselage's internal capacity, is given by:

$$V = \frac{\pi l d^2}{6}$$

Because parasite drag encompasses the entire airframe, it is highly useful to compute an equivalent parasite area for each component. This standardizes the area by multiplying it with the reference wing area, allowing total drag to be expressed as a simple summation of these equivalent areas. For the fuselage, this equivalent area is:

$$A_{fuse} = [1 + 1.5(\frac{l}{d})^{-1.5} + 7(\frac{l}{d})^{-3}] * C_f S_{wet}$$

Following the fuselage, the wing is the next major contributor in the drag buildup. The equivalent parasite drag area and resulting drag force for the wing are calculated as:

$$D_{wing} = 2C_f S_{wing} q_\infty = A_{wing} q_\infty$$

Similar substitutions of the respective equivalent areas are used to find the drag contributions of the horizontal and vertical stabilizers. By summing the fuselage, wing, empennage, and auxiliary components (such as ruggedized landing gear struts required for gravel runways), the total parasite drag of the aircraft is formulated:

$$D_o = (A_{fuse} + A_{wing} + A_{h-tail} + A_{v-tail} + A_{aux}) q_\infty$$

The total parasite drag coefficient is simply this summated area divided by the reference wing area:

$$C_{D,o} = \frac{(A_{fuse} + A_{wing} + A_{h-tail} + A_{v-tail} + A_{aux})}{S}$$

With the parasite drag coefficient defined, the induced drag coefficient is calculated based on the aircraft's lift and wing geometry. Induced drag is particularly vital for a STOL aircraft, which demands extreme lift generation at low speeds during short-field approaches. The induced drag coefficient is:

$$C_{D,i} = \frac{C_L^2}{\pi e AR}$$

A unique consideration for an Arctic STOL aircraft taking off and landing on unprepared fields is the substantial reduction in induced drag caused by Ground Effect. This aerodynamic phenomenon is captured by the nondimensional coefficient ϕ, expressed as:

$$\phi = \frac{(16\frac{h}{b})^2}{1 + (16\frac{h}{b})^2}$$

where h is the wing's height above the ground and b is the wingspan. This coefficient is multiplied by the induced drag to accurately reflect performance gains near the runway surface.

Finally, the overall aerodynamic efficiency of the aircraft is captured by the maximum Lift-to-Drag Ratio (E_{max}). This metric is absolutely critical for optimizing the 450-nmi cruise segment and maintaining the required 45-minute endurance loiters typical of emergency medical flights. Utilizing the previously determined baseline parasite drag coefficient, E_{max} is given by:

$$E_{max} = \sqrt{\frac{1}{4kC_{D,o}}}$$

2.4 Propulsion Characteristics

The propulsion system of choice for the Borealis aircraft consists of two PT6A-60A turboprop engines. For a turboprop aircraft operating across a wide range of altitudes, the shaft power available P_A is heavily dependent on the ambient atmospheric density. This relationship is modeled by scaling the sea-level power available ($P_{A,SL}$) by the local density ratio:

$$P_A = P_{A,SL} \cdot \sigma$$

The actual thrust power delivered to the airframe to counteract aerodynamic drag is governed by the propeller efficiency (η_p). This efficiency dictates the translation of shaft power into useful propulsive power, forming the core of the thrust-matching equations utilized during mission simulations.

2.5 STOL Takeoff and Landing Performance

Takeoff:

One of the most extreme design constraints imposed on the Borealis aircraft is the requirement to execute both takeoff and landing within a strictly limited 500 ft field length while safely clearing a standard 50 ft obstacle (h_{obs} = 50 ft). Operating in austere Arctic environments further complicates this metric, as the aircraft must routinely depart from rough, unpaved gravel or ice runways.

To accurately model the takeoff ground roll (d_{ground}) without relying on continuous numerical integration, the aircraft's acceleration is evaluated using a constant-force approximation. First, the available thrust must be defined. The static thrust for each PT6A engine is confirmed to be T_{static} = 1916.14 lbf (8.52 kN). With a twin-engine configuration, the total static thrust is simply:

$$T_{static,total} = 2 \cdot T_{static,each}$$

For the constant-force ground roll approximation, the average thrust (T_{av}) available during the dynamic takeoff run is estimated as 75% of the total static thrust:

$$T_{av} = 0.75 \cdot T_{static,total}$$

The net accelerating force, referred to here as the retarding force denominator (F_{ret}), balances this average thrust against the aerodynamic drag (D), lift (L), and the rolling friction of the Arctic surface (μ_r). These aerodynamic forces are evaluated at a dynamic pressure corresponding to 70% of the liftoff velocity ($0.7\ V_{LO}$). The retarding force is defined as:

$$F_{ret} = T_{av} - [D + \mu_r(W - L)]$$

With the liftoff velocity defined by a standard safety margin above stall ($V_{LO} = 1.2 * V_{stall}$) , the total ground roll distance can be calculated as:

$$d_{ground} = \frac{1.44W^2}{g\rho SC_{L,max}F_{ret}}$$

Once airborne, the distance required to clear the 50 ft obstacle d_{air} relies on the maximum steady climb angle (Θ_{max}) achieved at liftoff. The sine of this maximum climb angle is a function of the excess average thrust relative to the aircraft's instantaneous weight:

$$\sin(\theta_{max}) = \frac{T_{av} - D}{W}$$

$$\theta_{max} = \arcsin(\sin(\theta_{max}))$$

The airborne distance to clear the obstacle is then geometrically defined as:

$$d_{air} = \frac{h_{obs}}{\tan(\theta_{max})}$$

Landing:

Landing performance is modeled using an energy-based approach that critically accounts for both the steady approach glide and the dynamic flare maneuver prior to touchdown. The aircraft approaches the runway at a safe velocity of $V_A = 1.3\ V_{stall}$. The landing airborne distance covered from crossing the 50 ft obstacle to the moment of touchdown ($d_{air,landing}$) is approximated as:

$$d_{air,landing} = \left(\frac{L}{D}\right)\left[15 + \frac{0.133V_{stall}^2}{2g}\right]$$

Following touchdown, the aircraft must decelerate rapidly. Mirroring the takeoff approximation, the landing braking ground roll ($d_{landing}$) is evaluated at 70% of the touchdown velocity ($0.7\ V_{TD}$

). A specific landing retarding force ($F_{ret,landing}$) is defined to account for aerodynamic braking, wheel friction, and any reverse thrust (T_{rev}) generated by the turboprops:

$$F_{ret,landing} = D + \mu_r(W - L) - T_{rev}$$

Assuming maximum braking effort, the stopping distance is calculated utilizing the 1.69 energy factor:

$$d_{landing} = \frac{1.69W^2}{g\rho S C_{L,max} F_{ret,landing}}$$

By utilizing these exact, mirrored analytical formulations in the sizing loop, the design guarantees that the total takeoff distance ($d_{ground} + d_{air}$) and total landing distance ($d_{air,landing} + d_{landing}$) remain strictly under the 500 ft requirement for all payload configurations.

2.6 Climb Performance

To safely clear the 50 ft obstacle and depart the rough-field Arctic runways, the aircraft must maintain a sufficiently high climb gradient. The power required (P_R) for a propeller-driven aircraft in steady, unaccelerated flight is calculated by substituting the parabolic drag polar into the power equation:

$$P_R = \frac{1}{2}\rho V^3 S C_{D,0} + \frac{2KW^2}{\rho V S}$$

This equation demonstrates that during high-speed flight, parasite drag is the dominant factor, whereas induced drag becomes the primary power sink during low-speed STOL climb operations. The specific Rate of Climb (ROC) is dictated by the excess specific power available to the aircraft:

$$ROC = \frac{P_A - P_R}{W}$$

This relationship is evaluated continuously throughout the climb simulation to ensure that the aircraft maintains a sufficient climb rate to safely depart the Arctic environment under all payload configurations.

2.7 Mission Simulation: Range, Endurance, and Weight Fractions

The Arctic mission profiles demand complex tracking of the aircraft's weight as fuel is consumed across outbound flights, medical patient loading, and inbound returns. To account for this, a weight fraction analysis is embedded into the simulation, updating the instantaneous weight iteratively across each mission segment.

For a propeller-driven aircraft operating under standard FAR certification profiles, which typically dictate constant altitude and constant velocity (h, V constant) cruise segments, the required lift coefficient must decrease as fuel is burned, which alters the aerodynamic efficiency dynamically. The range for these constant h, V segments ($X_{h,V}$) is mathematically modeled utilizing the appropriate analytical Breguet formulation:

$$X_{h,V} = \frac{2\eta_p}{c_p} E_{max} \arctan\left(\frac{W_0^*\zeta}{1 + W_0^{*2}(1-\zeta)}\right)$$

where c_p is the specific fuel consumption, η_v is the propeller efficiency, ζ is the fuel weight fraction for the segment, and W_0* is the characteristic non-dimensional weight ratio. The continuous reduction in fuel weight throughout the mission is continuously updated in the performance model, and the total required fuel weight (W_f) is determined, including mandated reserves:

$$W_f = (1 + Reserve)(W_{takeoff} - W_{landing})$$

For this section, we used these equations early on for estimates, but later simulated the entire mission and fuel consumption over: climb to 9 km, cruise at 9 km (constant throttle), and descent to sea level. This was done iteratively, alongside takeoff and landing math, to find the correct fuel load for the mission

2.8 Stability and Control

To guarantee that the Borealis aircraft maintains safe and controllable flight characteristics across the entire mission envelope, preliminary stability and control assessments were conducted. The center of gravity (h_{cg}) fluctuates considerably due to the extreme variations in payload loading between the passenger, cargo, and medevac configurations. Longitudinal static stability requires that the aircraft's neutral point (h_{np}) remain aft of the center of gravity under all possible loading scenarios. This is quantified by computing the static margin (SM):

$$SM = \frac{h_{np} - h_{cg}}{c}$$

where c is the mean aerodynamic chord. A positive static margin was strictly maintained throughout the geometric design process. Furthermore, directional and pitch stability were guaranteed by appropriately sizing the empennage, which relies on the calculation of the horizontal and vertical tail volume ratios (V_h and V_v):

$$V_h = \frac{S_h l_h}{Sc} \quad ; \quad V_v = \frac{S_v l_v}{Sb}$$

where S_h and S_v are the respective tail areas, and l_h and l_v are the moment arms extending from the center of gravity to the aerodynamic centers of the tail surfaces.

2.9 Turning Performance

While the Arctic STOL aircraft is primarily optimized for short-field operations and robust cruising in harsh northern environments, turning performance remains a vital flight characteristic. Navigating through turbulent weather patterns, executing tight maneuvers during emergency Medevac approaches, or flying loiter patterns demands a comprehensive understanding of the airframe's turning capabilities.

For an unaccelerated turn, where both altitude and velocity are held strictly constant, the load factor is defined mathematically as the ratio of lift to weight. This foundational relationship is expressed as:

$$n = \frac{L}{W} = \frac{L}{D}\frac{T}{W}$$

where n is the load factor, W is the gross weight of the aircraft, T_A is the available thrust, and D is the aerodynamic drag. Although this relation might superficially imply that thrust equals drag during a turn, this is not accurate; executing a turn inherently necessitates an increase in required thrust to maintain the aircraft's velocity and altitude. The relationship governing the turning radius and dynamic pressure is subsequently obtained from:

$$r = \frac{2q}{\rho g \sqrt{n^2 - 1}}$$

where r represents the turning radius, q is the dynamic pressure, g is the constant of gravitational acceleration, and ρ represents the ambient air density.

The structural integrity of the airframe imposes a rigid physical boundary on the aircraft's maneuverability. By substituting the maximum permissible structural load factor into the radius equation, the limitation imposed by the airframe on the minimum turn radius is determined as:

$$r = \frac{2q}{\rho g \sqrt{(n_{struct})^2 - 1}}$$

where n_{struct} dictates the ultimate structural limit load factor the Arctic aircraft can safely sustain without suffering airframe damage.

Beyond structural constraints, the turning radius is heavily restricted by the aerodynamic stall boundary, which is directly tied to the maximum lift coefficient of the chosen airfoil. To prevent an accelerated stall during a banking maneuver, the lift coefficient constraint is defined by:

$$C_{Lmax} = \frac{L}{qS} = \frac{nW}{qS}$$

By integrating this lift coefficient limitation with the fundamental turn radius equation, the effect of aerodynamic limits on the turning radius is found. This combination yields:

$$r = \frac{2q(W/S)}{\rho g \sqrt{(C_L q)^2 - (W/S)^2}}$$

This expression illustrates how the relatively large wing area and resulting wing loading (W/S) of the STOL aircraft heavily influence its tight turning capabilities before encountering an aerodynamic stall.

The third and final major limitation on turning performance is dictated by the aircraft's propulsion system. The balance between power available and power required during an extended turn is modeled as:

$$P_A V = P_R V = C_{D0} qS + \frac{n^2 W^2}{qS\pi eAR}$$

where P_A is the power available from the wing-mounted engine configuration and P_R is the power required to sustain the maneuver. The maximum sustainable load factor constrained strictly by power limitations, denoted as n_{power}, is extracted from this energy relationship:

$$n_{power} = \left[(P_A V) - (C_{D0} qS) \frac{qS}{kW^2} \right]^{\frac{1}{2}}$$

where the aerodynamic constant k is dependent on the aircraft's spanwise efficiency and is given by the relation:

$$k = \frac{1}{\pi e AR}$$

Finally, combining the power-limited load factor with the fundamental turn radius equation yields the final turning constraint. This represents the tightest turn the aircraft can sustain without losing airspeed or altitude due to power deficiency:

$$r = \frac{2q}{\rho g \sqrt{(n_{power})^2 - 1}}$$

In later sections, these three limiting conditions—maximum lift coefficient, structural limit load, and power available will be used to construct comprehensive r-q diagrams. In order to actually carry out the necessary loiter patterns and turning maneuvers for the design missions, the power available must be accurately determined to account for these thrust-limiting n_{power} turning radius values.

2.9 Computational Design Flow

The theoretical foundations detailed in the previous sections were integrated into a comprehensive sizing loop. Computational scripts developed in MATLAB, coupled with 2D and 3D aerodynamic data generated via XFOIL and AVL, formed the core of the iterative design process. The algorithm continuously steps through each phase of the RFP mission profile, recalculating the drag polar, required engine power, and fuel weight fractions. By converging on the gross takeoff weight iteratively, the computational flow ensures that the final aircraft geometry strictly satisfies all aerodynamic, propulsive, and structural constraints imposed by the harsh Arctic environment.

Chapter 3

Results

3.1 Configuration and Selection Overview

The overall aircraft configuration was selected to meet the unique operational requirements of Arctic Short Takeoff and Landing (STOL) missions, including operation from both paved and unpaved surfaces, extreme ambient temperature conditions, and the need for flexibility across multiple mission types. The final configuration includes a high-wing, twin-turboprop layout with a cruciform tail and retractable tricycle landing gear, representing a synthesis of proven design practices and mission-specific tradeoffs.

The design process began with a broad survey of candidate configurations, including the following traits of aircraft design; low-wing vs. high-wing layouts, single vs. twin-engine propulsion, and type of propulsion system. These options were evaluated qualitatively based on their ability to meet key requirements. The final configuration was selected based on its ability to best satisfy these constraints simultaneously.

Requirement Category	**Design Requirement**	**Implication for Aircraft Design**
STOL Performance	Takeoff and landing distance ≤ 500 ft (152 m)	Requires high $C_{L,max}$, large wing area, and high thrust-to-weight ratio
Runway Capability	Operation from gravel and unprepared surfaces	High-wing configuration, robust landing gear, large low-pressure tires
Mission Flexibility	Passenger, cargo, and medevac configurations	Large fuselage volume and modular internal layout
Arctic Reliability	Operation in remote, extreme cold environments	Twin-engine redundancy, turboprop propulsion, cold-weather systems

Table 3.1.1. Mission Requirements and Design Implications

A high-wing configuration was selected due to its advantages in both aerodynamic performance and operational practicality. By positioning the wing above the fuselage, the design achieves increased ground clearance for propellers and engine nacelles, reducing the risk of foreign object debris ingestion when operating on gravel surfaces. This is a critical requirement for Arctic operations, where runway conditions are often poor or variable.

Additionally, the high-wing layout improves pilot visibility during approach and landing and allows for unobstructed cabin space below the wing, simplifying internal arrangement for passenger, cargo, and air ambulance configurations.

The aircraft employs a twin turboprop propulsion system, using two Pratt & Whitney Canada PT6A-60A engines, each producing approximately 772 kW of shaft power. This configuration was selected over jet propulsion due to the superior low-speed thrust characteristics of turboprops, which are essential for STOL performance.

At low velocities, turboprops generate higher thrust relative to jet engines due to the inverse relationship between thrust and velocity:

$$T = \frac{\eta P}{V}$$

where T is thrust, η is the propeller efficiency, P is the shaft power available, and V is the aircraft velocity.

This makes them particularly well suited for takeoff and climb segments. Furthermore, turboprops offer higher propulsive efficiency at the moderate cruise speeds required for the mission, improving fuel economy which directly impacts operating life cycle cost.

The twin-engine configuration also provides redundancy, enhancing safety for operations over remote terrain where diversion options are limited. This redundancy is considered essential for certification and practical operation in Arctic environments.

The initial wing geometry was derived from scaling existing STOL aircraft such as the Canadair CL-415 and DHC-6 Twin Otter, which exhibit similar mission profiles and operational constraints.

Parameter	**Value**	**Units**
Wing Span	28.6	m
Mean Aerodynamic Chord	3.5	m
Wing Area	100.1	m^2
Aspect Ratio	8.2	–

Table 3.1.2 Wing Configuration Parameters Table

This relatively large wing area is necessary to reduce stall speed and meet the stringent takeoff distance requirement. The aspect ratio was selected to balance induced drag reduction.

The fuselage was designed to accommodate three mission configurations: passenger transport, cargo transport, and aerial ambulance. These three internal requirements drove a relatively large fuselage cross-section, resulting in an external diameter of approximately 2.911 m and a length of approximately 16.7 m.

The fuselage geometry reflects a compromise between internal volume and aerodynamic efficiency. While a smaller fuselage would reduce parasite drag, it would not provide sufficient space for cargo and medical operations. Therefore, the design prioritizes operational flexibility and usability over minimal drag.

A cruciform tail was selected to improve tail effectiveness while avoiding the weight, structural complexity, and deep-stall risks of a full T-tail. It provides better clearance from the fuselage, wing wake, and ground effects than a low-mounted conventional tail, while remaining simpler and more reliable than a T-tail.

A retractable tricycle landing gear configuration was selected to balance aerodynamic efficiency and operational capability. While fixed landing gear would simplify design and improve robustness, retractable gear reduces drag during cruise, improving range and fuel efficiency.

The landing gear system is designed to withstand operations on gravel and unprepared surfaces, with appropriate structural reinforcement and oversized low-pressure tires selected to handle takeoffs and landings on unprepared fields.

3.2 Mission Configurations and Internal Arrangement

The aircraft was designed to be reconfigurable with distinctive constraints for passenger transport, cargo transport, and aerial ambulance. Each configuration imposes different constraints on payload, cabin layout, and accessibility, making the internal arrangement a primary driver in fuselage sizing and structural design.

The design objective was to create a single airframe capable of rapid reconfiguration between these constraints without requiring significant structural modification. This requirement was a key factor for designing the fuselage cross-section, cabin length, and internal systems layout.

Configuration 1: Passenger transport

The aircraft is required to carry:

- 9 passengers / 2,250 lb (200 lb + 50 lb baggage per passenger)
- 2 crew members / 400 lb (180 lb each + 20 lb baggage per pilot)

To meet the minimum seating requirement of 31-inch seat pitch, the total cabin seating length was estimated as:

$$L_{cabin} = 9 * 0.8128 = 7.1\,m$$

A single-aisle configuration with dual-side seating was selected to balance passenger capacity and accessibility. This arrangement is a typical seating arrangement for a passenger plane, which has been proven to provide adequate aisle width for movement and evacuation, efficient boarding and deplaning, and compatible cargo layouts.

The high-wing configuration allows unobstructed cabin space, since the wing spar does not intrude into the passenger compartment. This simplifies the seating layout and improves comfort.

Configuration 2: Cargo transport

The cargo configuration requires the aircraft to carry an equivalent payload mass to the 9 pax configuration while accommodating large and irregularly shaped objects. It also required carrying an 8,000 W generator and storing 55 gallons of diesel fuel

Based on the generator dimensions and required clearance, the minimum internal floor width was determined to be approximately $W_{floor} \approx 1.7\ m$. The floor width accounts for equipment footprint, loading clearance, and aisle space for personnel. The cargo configuration drove the fuselage diameter selection, as a narrower fuselage would not accommodate the required equipment. Additionally, a reinforced floor structure is required to support concentrated loads from heavy equipment.

Configuration 3: Aerial Ambulance

This configuration introduces additional spatial and operational constraints due to the need for medical access and patient transport. The requirement for the configuration includes: 1 stretcher (50 lb), 4 occupants (patient, escort, 2 medical personnel), 300 lb of medical equipment, and a total payload (1,150 lb).

This configuration places a strong constraint on fuselage diameter and door design. The cabin must allow medical personnel to work effectively during flight, which necessitates a wider cross-section than a passenger aircraft.

A key design requirement is the ability to transition between configurations quickly and efficiently. This is particularly important for Arctic operations, where a single aircraft may be required to perform multiple roles within short timeframes.

The aircraft is designed with a modular interior system, allowing quick removal of passenger seats and installation of cargo-carrying equipment. Cabin furniture, including passenger seats, stretcher mounts, cargo restraints, and medical equipment supports, is mounted to rail tracks in or on the floor. These rails allow interior components to be repositioned, removed, or locked into alternate layouts without major structural modification. Passenger seating is designed to be removable in sections, enabling rapid conversion to cargo or aerial ambulance layouts. The use of standardized mounting points ensures compatibility across all configurations. Turnaround time between configurations is estimated to be within one hour for full reconfiguration.

3.3 Sizing and Weight Estimation

Historical data, analytical scaling relationships, and performance simulations were used during the process of sizing and weight estimation of our aircraft. With a focus on cargo capacity, STOL performance, and range capabilities, the goal was to create a standard set of aircraft dimensions and weight that meet the main mission criteria.

The total weight of the aircraft is calculated by

$$W_0 = W_{OEW} + W_{payload} + W_{fuel}$$

where W_0 is the maximum takeoff weight, W_{OEW} is the operating empty weight, $W_{payload}$ is the mission payload, and W_{fuel} is the fuel weight.

For the initial estimates for the empty weight fraction (EWF) of our aircraft, historical data from comparable design characteristics of twin turboprop propulsion, mission capability, and high wing layouts. The referenced aircraft were DHC-6 Twin Otter, Canadair CL-415, and Short 330/360. For the referenced group of aircraft, the operating EWF range from

$$EWF = \frac{W_{OEW}}{W_0} \approx 0.62 - 0.68$$

Based on this comparison, an initial EWF of approximately 0.62 was selected as the baseline sizing value. This value was chosen due to our aircraft requiring a twin-engine turboprop configuration and a large wing and fuselage to meet the mission requirements.

Throughout refining our aircraft, the empty weight fraction was adjusted to account for major weight drivers specific to the Arctic STOL missions, which include larger wings for low-speed lift, reinforced landing gear, and additional FIKI systems for icing protection. The range for this aircraft's missions is also significantly lower than the contemporaries referenced before, so the takeoff fuel requirement decreased significantly. As a result, the final design uses an estimated EWF of approximately 0.74–0.76

The final aircraft weight was determined through iterative analysis and simulation, converging to a maximum takeoff weight of approximately 58.5 kN.

The overall weight breakdown is summarized as follows:

The operating Empty Weight (OEW) is calculated as

$$W_{OEW} \approx 0.76 \times 58.5 \approx 44.46\ kN$$

which includes the fuselage and wing structure, engines, landing gear, and avionics.

Configuration	Payload ($W_{payload}$) [kN]	Fuel Weight (W_{fuel}) [kN]
Passenger (9 passengers + baggage and crew)	10	3.77
Cargo	10	3.77
Aerial Ambulance	5.1	6.10

Table 3.3.1. Summarizes the payload and fuel allocation for each mission configuration at the final maximum takeoff weight of 58.5 kN

W_{fuel} was calculated using

$$W_{fuel} = W_0 - W_{OEW} - W_{payload}$$

This configuration allows increased fuel capacity due to reduced payload weight, improving range and endurance.

The fuel storage was mainly allocated in the wing, where 70% of the wing volume is available for fuel. The volume significantly exceeds the fuel required for the mission, allowing all required fuel to be stored within the wing structure. As a result, additional fuselage fuel tanks are not required, which helps preserve cabin space for the passenger, cargo, and medevac configurations. Locating the fuel in the wings also improves overall center-of-gravity stability because the fuel mass remains closer to the aircraft's aerodynamic center and reduces large CG shifts as fuel is burned throughout the mission.

3.4 Fuselage Design

The design of the fuselage focused on three primary objectives: Accommodating mission configurations, minimizing aerodynamic drag, and providing structural integrity. Due to having multiple requirements, the fuselage design was largely driven by internal volume constraints.

The cargo and medevac layouts, which are the most restricted configuration, were used to determine the fuselage cross-section dimensions. These configurations require sufficient floor width for large equipment and aisle clearance.

For the payload, dimensional constraints consist of a minimum internal floor width of 1.7m and require additional clearance for structure, wiring, and insulation

To account for structural thickness and system routing, the external fuselage diameter was defined as

$$D_{ext} = D_{int} + 0.10\, m$$

where the final external diameter resulted in being $D_{fus} = 2.91\ m$.

Regarding the circular cross-section, emphasis was kept on structural simplicity, stress distribution, and ease of pressurization. While non-circular cross sections could reduce drag, they would significantly complicate structural design and manufacturing.

The length of the fuselage was determined while considering the cabin length, tail moment arm, and aerodynamic considerations. Mission configuration constraints consist of passenger seating length needing to be 7.1 m, cockpit and systems, and tail moment arm. The length of our fuselage was selected to be $L_{fus} \approx 16.66\ m$. This length was chosen as it provides sufficient cabin volume, a reasonable distance between wing and tail for stability, and aerodynamic proportions.

The fuselage wetted area was calculated using CAD geometry, resulting in

$$S_{wet} \approx 129.06\, m^2$$

This large surface area makes the fuselage a dominant contributor to parasite drag. The Reynolds number for the fuselage at cruise conditions was estimated as

$$Re_{fus} \approx 1.31 \times 10^8$$

Using the turbulent flat-plate approximation

$$C_f = \frac{0.074}{Re^{1/5}} \approx 0.00176$$

This value was used in drag buildup calculations to determine the fuselage drag coefficient. The Fuselage structural weight was estimated using a surface-area-based method:

$$W_{fus} = (90\, N/m^2) \times S_{wet}$$

Substituting with actual values,

$$W_{fus} \approx 90\ *\ 129.06\ =\ 11.6\, kN$$

This makes the fuselage one of the largest contributors to the aircraft's empty weight.

3.5 Wing Design

The wing design was developed to satisfy the primary aerodynamic and performance requirements of the aircraft, with particular emphasis on STOL capability, lift generation, and aerodynamic efficiency. The wing must provide sufficient lift at low speeds to meet the 500 ft takeoff length constraint while maintaining acceptable drag characteristics for cruise and range performance.

Airfoil selection was driven by the need to maximize the maximum lift coefficient ($C_{L,max}$) while maintaining reasonable drag performance at cruise Reynolds numbers. Initial analysis was conducted using the NACA 2217 airfoil, which has a relatively high thickness-to-chord ratio (~17%), strong lift characteristics, and structural compatibility with fuel storage.

XFOIL analysis at the representative cruise Reynolds number, $Re = 2.78\times10^{7}$, produced

$$C_L = 0.726$$

$$C_D = 0.0055 \text{ at } \alpha = 2^{\circ}$$

However, AVL simulation revealed that the airfoil required a negative angle of attack for cruise lift balance, indicating excessive camber for the desired operating regime.

To address this, a modified airfoil, NACA 2417, was evaluated, reducing camber from 4% to 2%. This change improved cruise trim conditions and reduced unnecessary lift at low angles.

The wing planform was designed as a tapered trapezoidal wing to improve aerodynamic efficiency and reduce induced drag. The table below shows the final geometry metrics.

Parameter	Value	Units
Wing Span	28.6	m
Root Chord	3.89	m
Tip Chord	1.39	m
Wing Area	100.1	m^2
Aspect Ratio	8.17	–

Parameter	Value	Units
Sweep Angle	5	°
Dihedral Angle	0	°
Wing Incidence	2	°

Table 3.5.1. Final Wing Geometry Parameters

The taper ratio reduces wingtip loading and improves aerodynamic efficiency while maintaining manageable structural loads. The relatively large wing area was selected to reduce stall speed, enable short takeoff distances, and support a high payload at low speeds

The wing was analyzed using AVL (Athena Vortex Lattice) to evaluate lift distribution and induced drag characteristics. The results show an elliptical lift distribution with an Oswald efficiency factor of $e = 0.99$.

This extremely high efficiency indicates that the wing is close to an ideal lifting surface, minimizing induced drag. These results validate the chosen platform geometry and confirm that the wing design is aerodynamically efficient.

To meet the strict STOL requirement (≤ 500 ft takeoff distance), high-lift devices were incorporated into the wing design. Fowler flaps increase camber, effective wing area, and $C_{L,max}$. An empirical analysis, it shows that the baseline airfoil $C_{L,max}$ can increase up to 3.2 with Fowler flaps. This increase is critical, as stall velocity depends on

$$V_{stall} \propto \frac{1}{\sqrt{C_{L,max}}}$$

Without Fowler flaps, the aircraft cannot meet the 500 ft STOL requirement.

The wing also serves as the primary fuel storage location. Based on design assumptions, up to 70% of the wing volume is available for fuel storage. Given the selected wing geometry, sufficient volume exists to store all required mission fuel within the wing structure. As a result, the final design adopts wing-integrated fuel tanks as the primary fuel storage solution.

3.6 Propulsion System

Borealis uses a twin-turboprop propulsion system with two Pratt & Whitney Canada PT6A-60A engines mounted in wing nacelles. The PT6A family was selected because it is widely used in utility and regional aircraft, has a strong reliability history, and is well-suited for short-field operations where high low-speed thrust is required. Pratt & Whitney lists the PT6A family as ranging from 500 shp to over 1,900 shp, with broad use across many aircraft applications.

3.6.1 Engine downselect (PT6A-60A vs. PT6A-68C vs. alternatives)

Borealis uses two Pratt & Whitney Canada PT6A-60A turboprop engines. Each engine was modeled at 772 kW of sea-level shaft power, giving a total installed sea-level power of:

$$P_{SL,total} = 2(772) = 1544\ kW$$

3.6.2 Power available vs. altitude and temperature (ISA+5)

Available shaft power was corrected for altitude using the atmospheric density ratio:

$$P_A = P_{SL,total}\sigma$$

where P_A is the altitude-corrected shaft power, PSL,total is the total sea-level shaft power, and σ is the density ratio. For Borealis, the two PT6A-60A engines provide a total modeled sea-level shaft power of 1544 kW. At the 9 km cruise altitude used in the mission analysis, the density ratio was found to be
σ = 0.3805. Therefore,

$$P_A = 1544(0.3805) = 587.42\ kW$$

This value represents the available shaft power at 9 km before propeller efficiency is applied. Using the cruise propeller efficiency of $\eta_p = 0.80$, the effective propulsive power becomes

$$P_{prop} = 587.42(0.80) = 469.94\ kW$$

3.6.3 Propeller selection and efficiency assumptions

A constant-speed propeller system was assumed for Borealis to provide efficient operation across climb and cruise conditions. This configuration is appropriate for a turboprop STOL aircraft because it allows the propeller to maintain effective thrust during low-speed climb while still operating efficiently during cruise.

Different propeller efficiencies were applied for climb and cruise. During the climb, the propulsion model used

$$\eta_{p,climb} = 0.75$$

to represent the lower propeller efficiency associated with high-thrust, low-speed operation. During the cruise, the model used

$$\eta_{p,cruise} = 0.80$$

These values convert engine shaft power into usable propulsive power according to

$$P_{prop} = P_A \eta_P$$

At the 9 km cruise condition, the available shaft power was 587.42 kW. Therefore, the cruise propulsive power is

$$P_{prop,cruise} = 587.42(0.80) = 469.94\ kW$$

For comparison, using the climb propeller efficiency at the same shaft-power condition gives

$$P_{prop,climb} = 587.42(0.75) = 440.57\ kW$$

The lower climb efficiency represents the less efficient high-thrust, low-speed condition, while the higher cruise efficiency reflects improved propeller performance at higher forward speed. These assumptions were used to convert shaft power into usable propulsive power in the climb and cruise performance models.

3.6.4 Specific fuel consumption and mission fuel burn implications

Mission fuel burn was modeled using a power-based specific fuel consumption relationship. The assumed engine-specific fuel consumption was

$$SFC_P = 0.6\frac{lb}{hp*hr}$$

which was converted to SI units in the mission model as

$$SFC_P = 9.945 \times 10^{-7}\frac{N_{fuel}}{W \cdot s}$$

Fuel consumption during powered segments was then calculated using

$$\frac{\delta W_{fuel}}{\delta t} = - SFC_P \times P_{shaft}$$

where P_{shaft} is the shaft power used during the mission segment. This means fuel burn increases with both engine power setting and time spent operating at that power level.

For the reference mission, the aircraft was modeled with a takeoff weight of 58,500 N, with 3,951.4 N of available fuel. The simulation results showed that taxi used 64.5 N of fuel, climb used 807.4 N, cruise used 2299.7 N, and descent used 16.7 N. Therefore, the total fuel used before landing and reserve segments was

$$W_{fuel,used} = 64.5 + 807.4 + 2299.7 + 16.7 = 3188.3\ N$$

This corresponds to

$$\frac{3188.3}{3951.4}(100) = 80.69\%$$

of the available fuel load. These results show that the PT6A-60A provides sufficient mission power while keeping fuel use relatively low during the main reference mission segments. The largest fuel demands occur during climb and cruise, making propeller efficiency, cruise altitude, and throttle setting important drivers of total mission fuel burn.

3.6.5 Nacelle integration and drag contribution

The two PT6A-60A engines are integrated into wing-mounted nacelles to support the high-wing STOL configuration of Borealis. This layout provides propeller ground clearance for gravel and snow operations while keeping the fuselage cabin unobstructed for passenger, cargo, and medevac configurations.

The nacelles contribute to parasite drag by increasing the aircraft's wetted and frontal area. In the drag buildup, the nacelles were grouped with landing gear and auxiliary components using an equivalent drag area of

$$\Delta f = 0.02\ m^2$$

At the start-of-cruise condition, the mission model gave ρ=0.4661 kg/m^3 and V = 106.8428 m/s. The resulting dynamic pressure is

$$q = \frac{1}{2}\rho V^2 = \frac{1}{2}(0.4661)(106.8428)^2 = 2661.1\ Pa$$

The drag contribution from the nacelle, landing gear, and auxiliary equivalent drag area is therefore

$$D_{aux} = 2661.4(0.02) = 53.2\ N$$

The corresponding power required at cruise is

$$P_{aux} = D_{aux}V = 53.2(106.8428) = 5.68\ kW$$

This drag penalty is small compared with the total cruise propulsive power, but it is included because nacelle size directly affects cruise efficiency. The nacelles were therefore sized to balance engine installation, cooling, maintenance access, anti-icing provisions, and aerodynamic cleanliness. Because Borealis is designed for unprepared Arctic surfaces and operation down to −30◦F, the nacelle layout must also account for inlet protection and foreign object damage resistance.

3.7 Drag Buildup

3.7.1 Fuselage parasite drag (ellipsoid model, Re-based skin friction)

The fuselage parasite drag was estimated using the CAD-derived fuselage surface area and a Reynolds-number-based skin-friction approximation. The final fuselage geometry had a nose-to-tail length of 16.663 m, a diameter of 2.911 m, and a total fuselage surface area of 129.0583 m^2, including a 0.02 m^2 allowance for antennas and small external features.

Using the cruise drag-estimation condition, the fuselage Reynolds number was

$$Re_{fus} = 131,459,189$$

The corresponding turbulent skin-friction coefficient was estimated as

$$C_f = \frac{0.074}{Re^{1/5}} = 0.0017598$$

Using the ellipsoid-based fuselage drag model, the fuselage parasite drag coefficient based on the fuselage wetted area was

$$C_{D0,fus} = 0.002018$$

To include the fuselage drag contribution in the aircraft drag polar, this value was converted to the wing reference area:

$$C_{D0,fus,ref} = C_{D0,fus}\frac{S_{fus}}{S}$$

With S_{fus}=129.0583 m^2 and S=28.6(3.5)=100.1 m^2,

$$C_{D0,fus,ref} = (0.002018)\frac{129.0583}{100.1} = 0.002602$$

3.7.2 Wing parasite drag

The wing parasite drag was estimated using the final wing reference geometry and a Reynolds-number-based skin-friction approximation. The selected wing has a span of 28.6 m and a mean chord of 3.5 m, giving a reference wing area of

$$S = bc = (28.6)(3.5) = 100.1\, m^2$$

The wing Reynolds number used in the drag estimate was

$$Re_{wing} = 27,849,183$$

Using the turbulent flat-plate skin-friction approximation,

$$C_f = \frac{0.074}{Re^{1/5}}$$

The wing skin-friction coefficient becomes

$$C_{f,wing} = \frac{0.074}{(27,849,183)^{1/5}} = 0.00240$$

After accounting for the airfoil geometry and wing form effects, the wing parasite drag contribution used in the aircraft drag buildup was

$$C_{D0,wing} = 0.0016$$

This value was combined with the fuselage parasite drag, empennage drag, landing gear, nacelle, and auxiliary drag terms to form the final aircraft parasite drag coefficient of

$$C_{D0,total} = 0.006363$$

which was used in the reference mission and performance simulations.

3.7.3 Empennage parasite drag

The empennage parasite drag was estimated from the horizontal and vertical tail planform areas. The horizontal tail was sized with a mean aerodynamic chord equal to half of the wing MAC and a span equal to 40% of the wing span. The vertical tail was modeled as having the same shape and size as half of the horizontal tail, with both tail surfaces using a symmetric NACA 0012 airfoil.

Using the final wing geometry,

$$b = 28.6\, m, c = 3.5\, m$$

The horizontal tail dimensions are

$$b_h = 0.4(28.6) = 11.44\, m$$

$$c_h = 0.5(3.5) = 1.75\, m$$

Therefore, the horizontal tail area is

$$S_h = b_h c_h = (11.44)(1.75) = 20.02\, m^2$$

The vertical tail area was taken as half of the horizontal tail area:

$$S_v = 0.5S_h = 0.5(16.1) = 8.05\, m^2$$

Thus, the total empennage reference area is

$$S_{emp} = S_h + S_v = 20.02 + 8.05 = 28.07\, m^2$$

The final aircraft reference area is

$$S = (28.6)(3.5) = 100.1\, m^2$$

For the final drag buildup, the empennage parasite contribution was included as

$$C_{D0,emp} = 0.001284$$

This value accounts for the parasite drag added by the horizontal and vertical stabilizers and was combined with the fuselage, wing, landing gear, nacelle, and auxiliary drag terms to form the final aircraft parasite drag coefficient used in the mission model. The final reference mission script uses

$$C_{D0,total} = 0.006368$$

for the complete aircraft parasite drag coefficient.

3.7.4 Landing gear, nacelles, and auxiliary contributions (0.02 m^2)

Landing gear, nacelles, and small auxiliary components were grouped into a single equivalent drag-area contribution. This included exposed landing gear effects, engine nacelle interference, antennas, probes, and other small external features. The project drag notes assign these auxiliary items a combined area contribution of

$$\Delta f_{aux} = 0.02\, m^2$$

Using the final wing reference area,

$$S = (28.6)(3.5) = 100.1\, m^2$$

The corresponding parasite drag coefficient contribution is

$$C_{D0,aux} = \frac{\Delta f_{aux}}{S}$$

$$C_{D0,aux} = 1.998 \times 10^{-4}$$

At the start-of-cruise condition, using $\rho = 0.4661\, kg/m^3$ and $V = 106.8428\, m/s$, the dynamic pressure is

$$q = \frac{1}{2}\rho V^2$$

$$q = \frac{1}{2}(0.4661)(106.8428)^2 = 2661.4\ Pa$$

The corresponding auxiliary drag force is

$$D_{aux} = q\Delta f_{aux} = 2661.4(0.02) = 53.2\ N$$

This contribution is small compared with the total aircraft drag, but it was included because exposed landing gear, nacelles, and small external features increase parasite drag and reduce cruise efficiency. The final reference mission model used the combined aircraft parasite drag coefficient

$$C_{D0,total} = 0.006368$$

which includes the auxiliary drag contribution along with the fuselage, wing, and empennage parasite drag terms.

3.7.5 Total C_{D0} and induced drag model

The induced drag term was modeled using the standard parabolic drag polar,

$$C_D = C_{D0} + kC_L^2$$

where k is the induced drag factor. The induced drag factor was calculated from

$$k = \frac{1}{\pi eAR}$$

Using the final wing geometry,

$$S = bc = (28.6)(3.5) = 100.1\ m^2$$

$$AR = \frac{b^2}{S} = \frac{(28.6)^2}{100.1} = 8.1796$$

$$e = 0.9877$$

The induced drag factor becomes

$$k = \frac{1}{\pi(0.9877)(8.1796)} = 0.03939$$

Therefore, the final drag model used for Borealis was

$$C_D = 0.006368 + 0.03939C_L^2$$

3.7.6 Drag polar and L/D characteristics

The final drag polar for Borealis was modeled using the parabolic drag relationship

$$C_D = C_{D0} + kC_L^2$$

The lift coefficient for maximum lift-to-drag ratio occurs when parasite and induced drag are equal:

$$C_{L,E_{max}} = \sqrt{\frac{C_{D0}}{k}} = \sqrt{\frac{0.006368}{0.03939}} = 0.40208$$

Under these conditions, the drag coefficient is

$$C_D = 0.006368 + 0.03939(0.40208)^2 = 0.0127$$

The maximum lift-to-drag ratio is then

$$E_{max} = (\frac{L}{D})_{max} = \frac{C_L}{C_D} = \frac{0.40208}{0.01274} = 31.57$$

Therefore, the final drag model predicts a maximum lift-to-drag ratio of

$$(\frac{L}{D})_{max} = 31.57$$

This value was used to evaluate cruise efficiency and mission range. The drag polar shows that parasite drag dominates at high speed, while induced drag becomes more important during low-speed climb, takeoff, and landing conditions.

3.8 Performance: Takeoff and Landing

Takeoff and landing performance were evaluated as primary design drivers because the aircraft must operate from short, unprepared Arctic runways. As the aircraft must take off and land over a 50 ft obstacle within 500 ft, the selection of wing area, high-lift devices, aircraft weight, and propulsion system is impacted.

The liftoff velocity was estimated using $V_{LO} = 1.2V_{stall}$, where the stall velocity is given by

$$V_{stall} = \sqrt{\frac{2W}{\rho S C_{L,max}}}$$

The takeoff ground roll was determined using a force balance including thrust, aerodynamic drag, lift-induced weight relief on the landing gear, and rolling resistance. Because the aircraft is designed for gravel and rough-field operations, rolling resistance was treated as a significant contributor to total takeoff distance.

With an initial takeoff weight of 121 kN, wing area of 80.5 m², and $C_{L,max} = 2.2$the resulting liftoff velocity is

$$V_{LO} = 40.1 \text{ m/s}$$

and a takeoff distance of approximately 562 m. This configuration failed to meet the 152 m requirement.

The results highlight the dominance of weight and lift coefficient in determining takeoff performance.

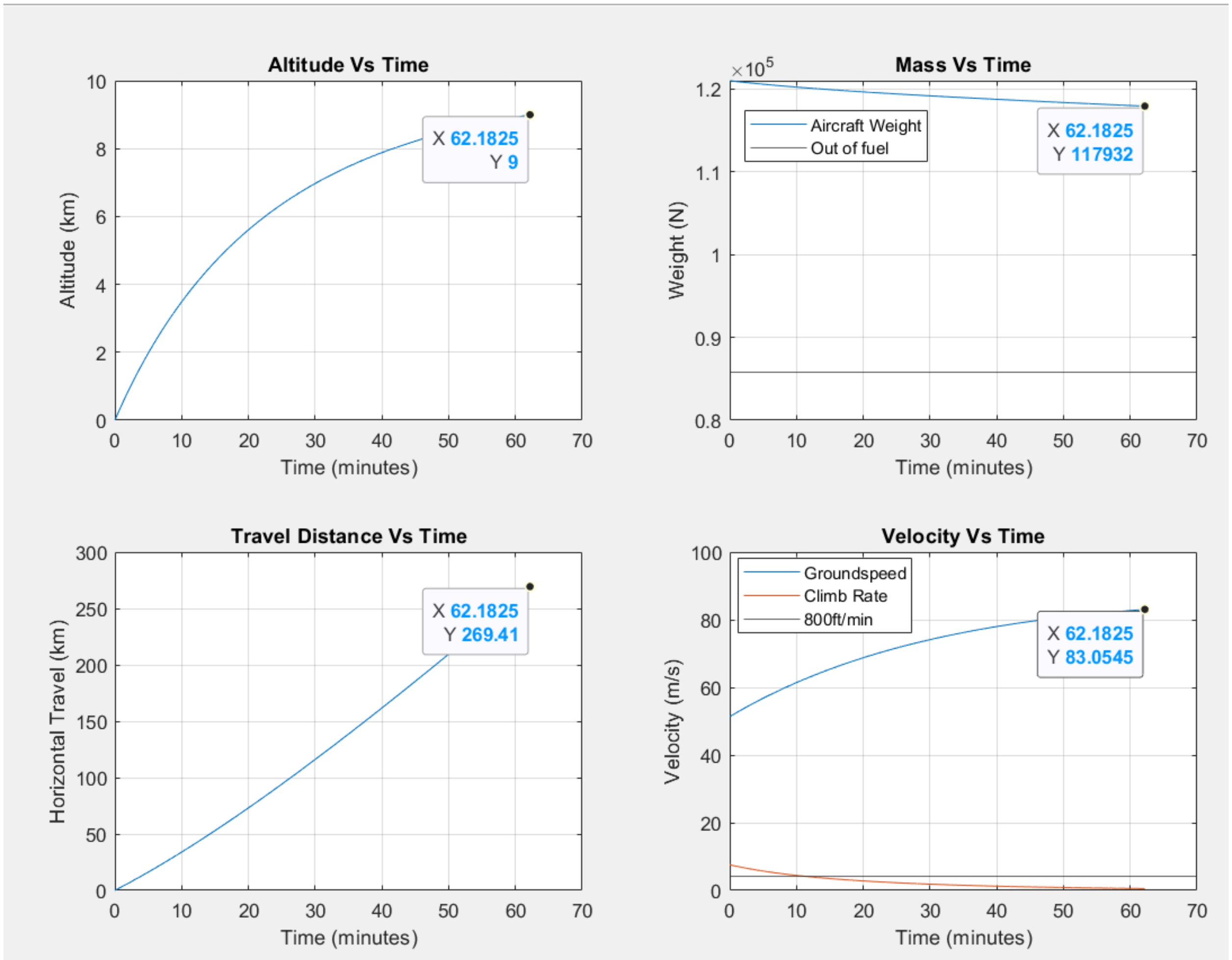

Figure 3.9.1. Takeoff distance breakdown for the baseline configuration

To address this limitation, the design was iteratively refined by reducing the aircraft's weight, increasing wing area, and incorporating high-lift devices. A Fowler flap system was selected due to its ability to increase both camber and effective wing area. The final configuration uses a wing area of 100.1 m², a maximum lift coefficient of approximately 2.4, and a reduced takeoff weight of 57.6 kN.

Under these conditions, the stall velocity reduced to around 32 m/s, resulting in a liftoff velocity of about 38.4 m/s. The reduction in stall and liftoff velocities significantly improves takeoff performance, enabling compliance with the 500 ft requirement.

Landing performance was evaluated similarly, where the touchdown velocity was estimated using

$$V_T = 1.3V_{stall}$$

which gave approximately 41.6 m/s for the final configuration. The total landing distance was separated into airborne distance from the 50 ft obstacle and ground roll after touchdown. The airborne portion depends primarily on glide slope and L/D, while the ground roll is governed by touchdown velocity, braking capability, aerodynamic drag, and rolling resistance.

For Arctic gravel operations, braking effectiveness and tire–surface interaction are critical due to reduced traction on loose or uneven surfaces. To provide additional landing margin, a tail-mounted drag parachute approximately 5 m in diameter was considered as a supplemental deceleration system. The aircraft may carry both a reusable parachute for established bases and a disposable unit for remote sites where recovery is impractical. This system would only be used when additional stopping capability is required.

Overall, the analysis shows that STOL performance is highly sensitive to aircraft weight, maximum lift coefficient, wing area, and available thrust. The original 121 kN configuration was not viable, but the final reduced-weight design with increased wing area, high-lift devices, and turboprop propulsion satisfies the 500 ft takeoff and landing requirement.

3.9 Performance: Climb

Climb performance was evaluated to verify compliance with the RFP requirement of a minimum rate of climb of 800 ft/min (4.06 m/s) at maximum takeoff weight under ISA+5 conditions. This requirement is critical for Arctic STOL operations, where the aircraft must rapidly clear obstacles after takeoff and safely depart remote, terrain-constrained runways.

The rate of climb was determined from the excess power relationship of

$$ROC = \frac{P_A - P_R}{W}$$

where P_A is the power available, P_R is the power required, and $W$is the aircraft's weight. The propulsion system consists of two PT6A-60A turboprop engines, providing a total sea-level shaft power of

$$P_{A,SL} = 2(772,000) = 1.544\times10^6 W.$$

A propeller efficiency of approximately 0.75 was used for climb conditions. Power available at altitude was reduced P_A to account for the degradation in engine performance with decreasing air density. Power required was computed using the drag model developed previously, incorporating both parasite and induced drag. Because climb occurs at relatively low velocities, induced drag plays a more significant role than in cruise.

For the final configuration ($W_0 = 57.6\,kN$), the simulation shows a maximum rate of climb of

$$ROC_{max} = 18.9\,m/s\ (3543\,ft/min)$$

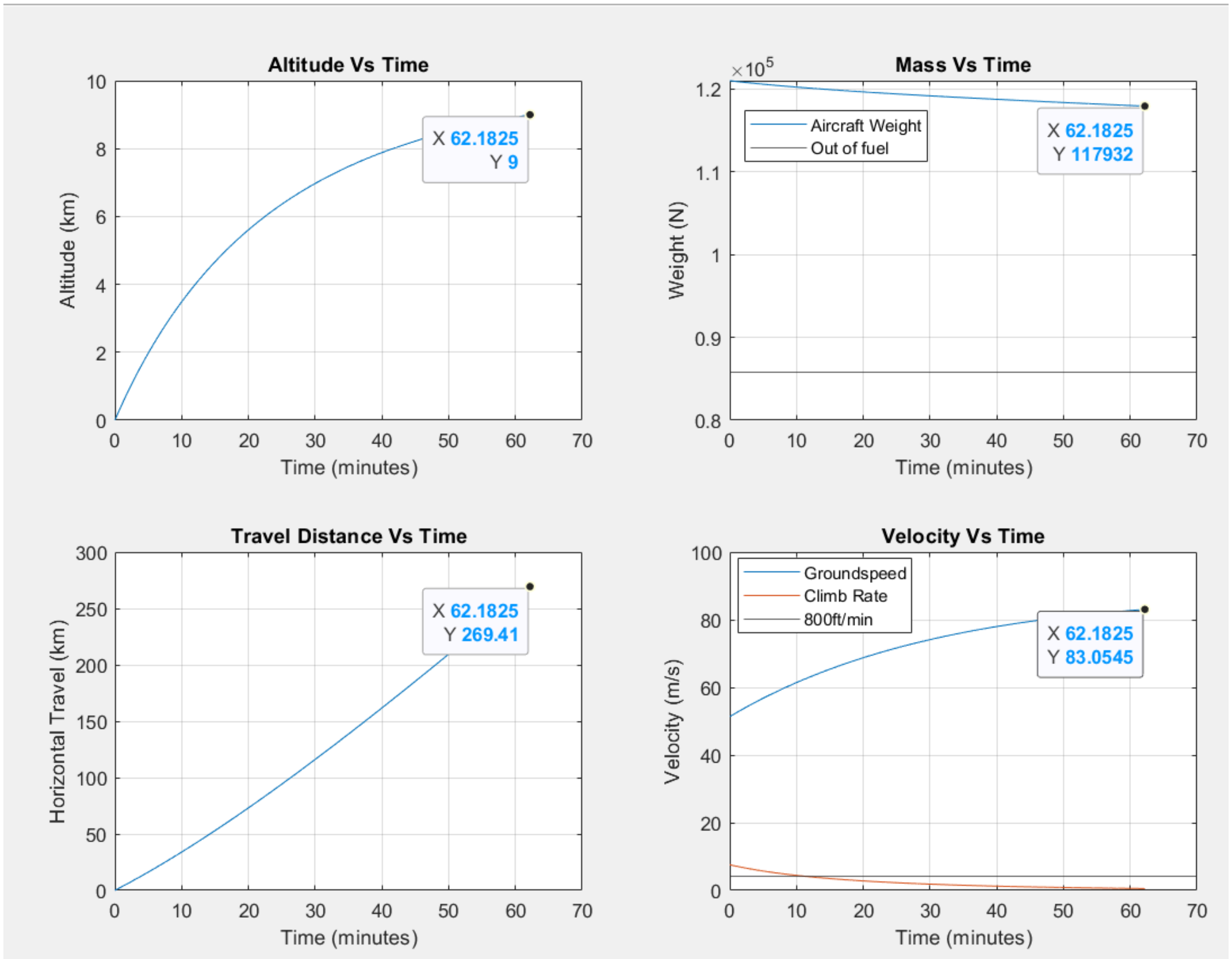

Figure 3.10.1. Climb performance results, including altitude, velocity, and horizontal distance as functions of time.

The aircraft reaches cruise altitude within approximately 60 minutes while maintaining a steadily increasing velocity profile.

3.10 Performance: Cruise

The cruise phase represents the most significant portion of the Arctic STOL aircraft's mission profiles, particularly for the 450 nmi reference mission and the dual-leg 350 nmi Medevac sorties. To maximize the operational efficiency and profit margins required by the mission objectives, the aircraft must be operated at conditions that balance fuel economy with the necessity for high average ground speeds. The cruise performance is characterized by the equilibrium where the power available from the twin PT6A-60A engines matches the power required to overcome the total aerodynamic drag at a specific altitude and velocity. For this air ambulance configuration, the cruise lift coefficient is established at 0.7263, which corresponds to a level flight state at an angle of attack determined through AVL characterization.

3.10.1 Optimal cruise altitude and velocity

Determining the optimal cruise condition requires a detailed trade study of how power requirements shift with density altitude and true airspeed. The power required (P_R) for the aircraft is derived from the total drag coefficient, which includes a parasite contribution (C_{D0}) of 0.006368 and an induced component dictated by the aspect ratio of 8.17 and an Oswald efficiency factor of approximately 0.99. According to Anderson, the power required is defined by the following relation:

$$P_R = \sqrt{\frac{2W^3C_D^2}{\rho S C_L^3}} = DV_\infty$$

Given the aircraft's maximum takeoff weight (MTOW) of 57,600 N and a wing area of 100.1 m^2, the power required is highly sensitive to the decreasing air density (ρ) at higher altitudes. As the aircraft climbs toward its service ceiling, the velocity for minimum power ($V_{P_{R,min}}$) and the velocity for minimum drag ($V_{D,min}$) both increase. For this design, the velocity at minimum drag at the start of the cruise is calculated to be 78.391 m/s.

The trade study identifies the optimal cruise point at the intersection of the power available (P_A) and power required curves. At the selected cruise altitude, the power available from the propulsion system, calculated as 1,544,000 W at sea level, is attenuated by the density ratio (σ) and the propeller efficiency (η), which is approximately 0.80 during cruise. The calculations show that at the target cruise velocity of 80 m/s (approx. 155 KTAS), the aircraft requires a shaft power of 125,570 W. This specific power requirement allows for a verification of the throttle settings, where the pilot maintains the required airspeed by adjusting the engine output to match the 2,155 N of drag experienced at cruise. By operating at these optimized conditions, the aircraft achieves an impressive maximum lift-to-drag ratio (E_{max}) of 31.55, ensuring that the mission range of 1,296.4 km can be met while still maintaining the necessary fuel reserves for a 45-minute loiter at best endurance speed.

3.10.2 Constant C_L vs. constant V vs. constant throttle comparison

Three idealized cruise control strategies were simulated at the design cruise altitude of 9 km, constant lift coefficient, constant velocity, and constant throttle, to characterize the trade between range, endurance, and transit speed for Borealis. Each mode imposes a distinct constraint on the equilibrium between weight, aerodynamic forces, and propulsive power, producing meaningfully different fuel-burn and distance characteristics.

Constant C_L Cruise

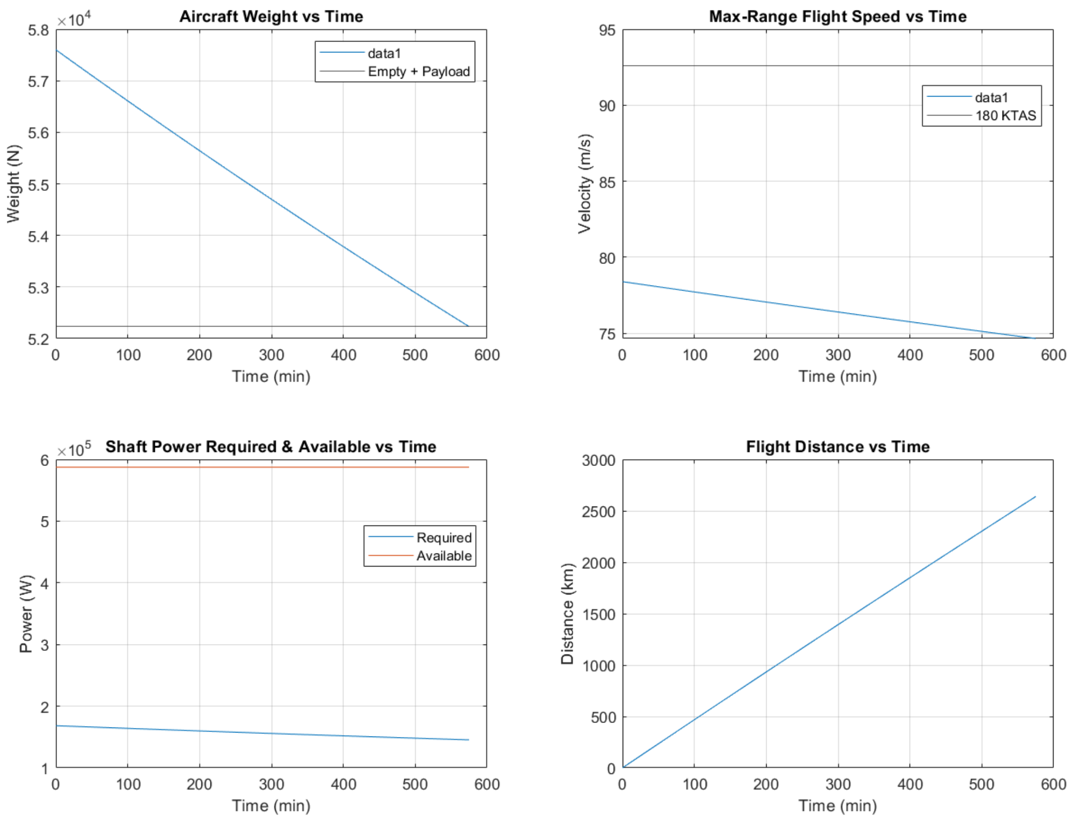

Holding the lift coefficient fixed at the maximum-range value of approximately 0.402, the cruise velocity is allowed to decay from roughly 78 m/s to 75 m/s as the aircraft's weight decreases from 57.6 kN to 52.4 kN over the 580-minute segment. The shaft power required falls correspondingly from approximately 1.6×10^5 W to 1.4×10^5 W, well below the 5.9×10^5 W available throughout the cruise. This mode most closely realizes the Breguet range-optimal condition for a propeller-driven configuration and produces the longest simulated flight distance, approximately 2,700 km, representing the theoretical upper bound on cruise range for the airframe.

Constant V Cruise

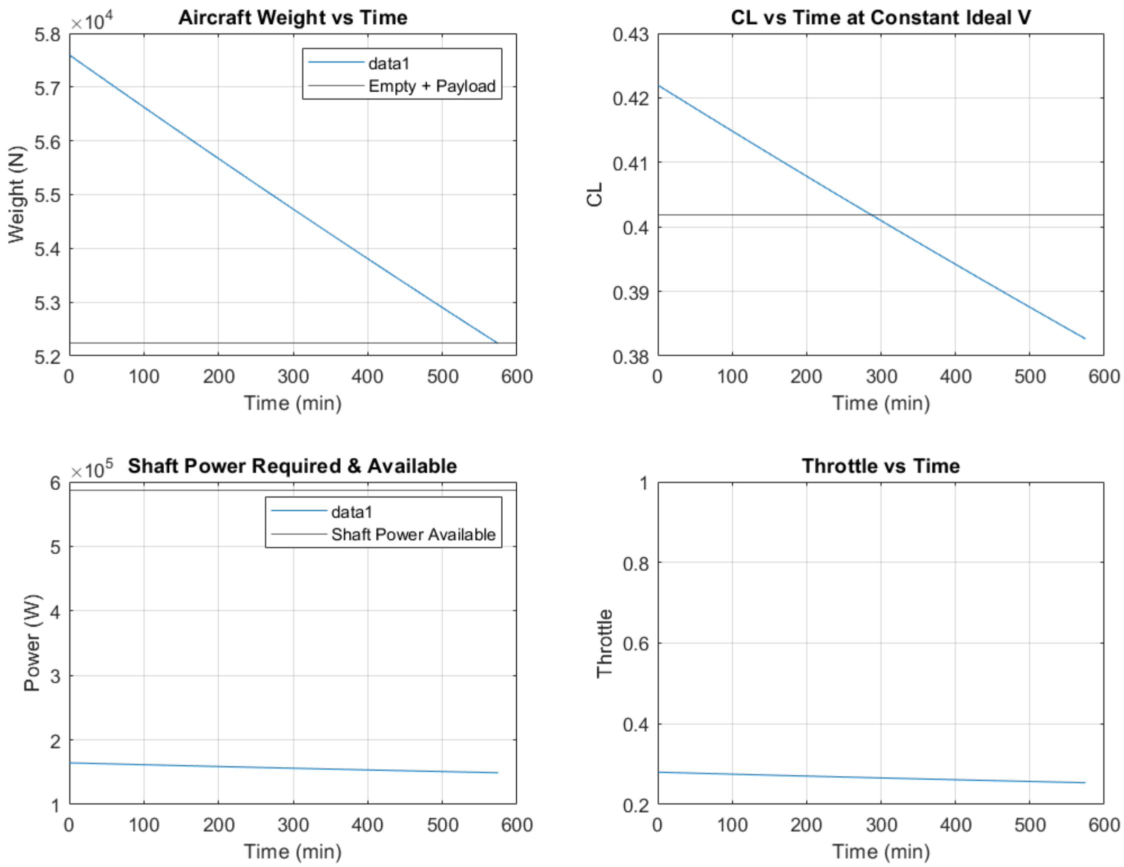

The constant-V profile fixes the cruise velocity near $V_{D,min} \approx 78.4$ m/s for the duration of the segment. As fuel is burned, the lift coefficient required to sustain level flight decreases monotonically from 0.422 to 0.382, passing through the optimal value of 0.402 near the midpoint of the cruise. Throttle setting reduces gradually from approximately 0.27 to 0.25, indicating that the aircraft operates with substantial excess power throughout. Because Federal Aviation Regulations mandate constant altitude and velocity for standard cruise, this mode represents the most operationally and regulatorily relevant baseline. The resulting range is essentially equivalent to the constant C_L case, with only a small penalty incurred by operating at off-optimal C_L during the early and late portions of the cruise.

Constant Throttle Cruise

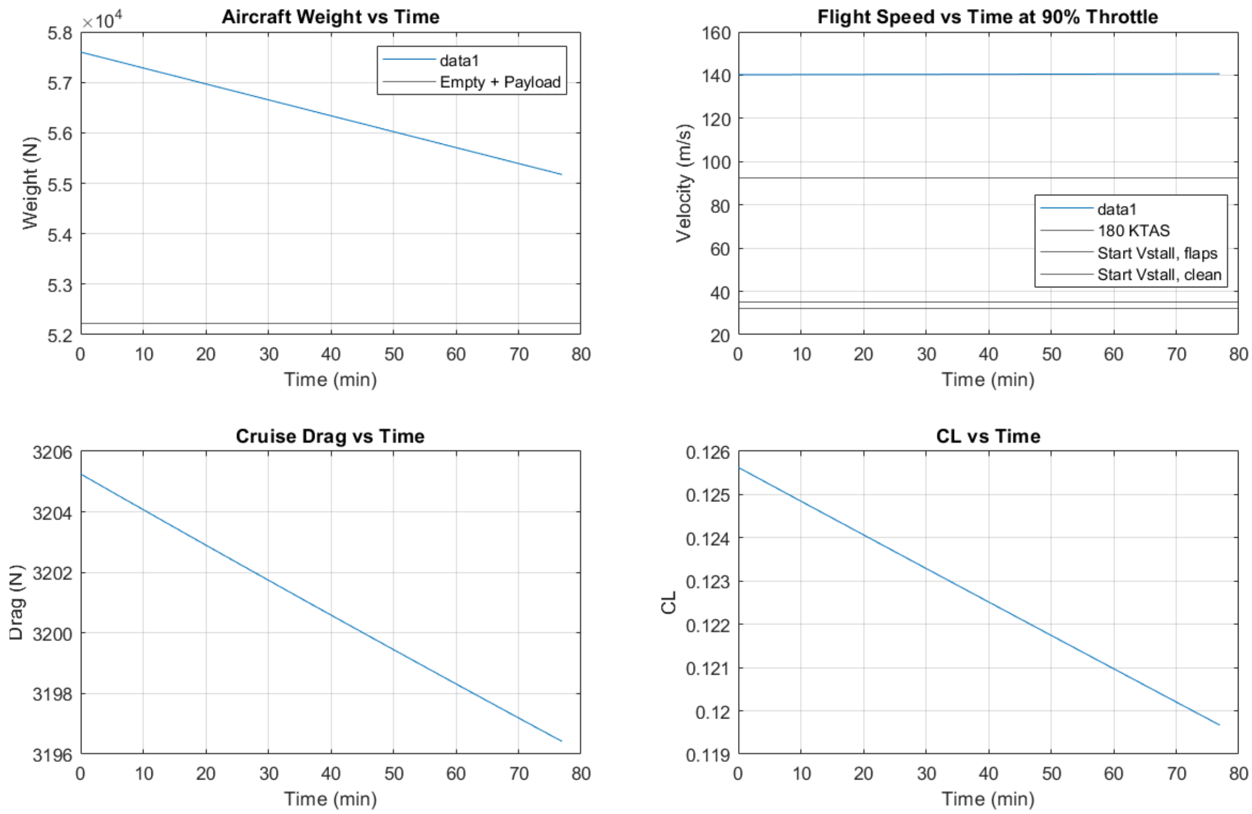

The constant-throttle simulation, executed at 90% throttle, stabilizes the aircraft at approximately 140 m/s, near the demonstrated V_{max} of 275.6 KTAS but well above the velocity for maximum aerodynamic efficiency. Cruise drag remains high at roughly 3,200 N, and the corresponding lift coefficient falls to about 0.12, substantially below the E_{max} value of 0.402. As weight decreases, the aircraft does not slow appreciably; instead, drag declines only marginally from 3,206 N to 3,196 N, and C_L decreases from 0.126 to 0.120. The elevated power demand drives a fuel burn rate roughly four times that of the C_L and V-based profiles, exhausting the equivalent fuel load in approximately 77 minutes and sharply reducing achievable range. While inefficient for long-range cruise, this mode is operationally relevant for time-critical medevac outbound legs, where minimum transit time outweighs fuel economy.

Comparison and Selection

The constant C_L profile yields the maximum theoretical range; the constant V profile delivers nearly identical performance under FAR-compliant procedures; and the constant-throttle profile sacrifices range and endurance for cruise speed. Borealis is therefore designed to cruise nominally at constant velocity near $V_{D,min}$, capturing the bulk of the constant C_L range advantage while preserving regulatory compliance, pilot workload simplicity, and a stable trim condition. The constant-throttle mode is retained as a contingency profile for high-priority medevac sorties where rapid patient transport is the dominant operational driver.

3.10.3 Throttle setting and SFC at cruise

Cruise fuel burn was calculated using the power-specific fuel consumption of the PT6A-60A turboprop engines. The given engine SFC was converted from

$$SFC_p = 0.6\frac{lb\,fuel}{hp * hr}$$

to SI units using

$$SFC_P = \frac{9.81(.453592)(.6)}{745.7(3600)}$$

which gives

$$SFC_P = 9.95 * 10^{-7}\ \frac{N_{fuel}}{W*s}$$

The available shaft power at altitude was reduced using the density ratio,

$$P_A(h) = P_{A,SL}\frac{\rho}{\rho_{SL}}$$

At the 9 km cruise altitude, the available shaft power was approximately

$$P_A \approx 5.9 * 10^5\,W$$

before applying the throttle setting. For the constant-velocity cruise case near $V_{D,min}$, the aircraft required only about 25–27% throttle. This corresponds to a shaft power requirement of approximately

$$P_{shaft} \approx 1.5 * 10^5\,W$$

The corresponding fuel burn rate is

$$W_{fuel} = SFC_P P_{shaft}$$
$$W_{fuel} = (9.95 * 10^{-7})(1.5 * 10^{5})$$
$$W_{fuel} \approx 0.15\ N/s$$

or approximately

$$540\ N/hr$$

This low throttle setting confirms that the aircraft has substantial excess cruise power when operating near the maximum-range speed. The 90% throttle case used much more of the available power and produced a significantly higher cruise speed, but at the cost of much higher fuel burn. At 90% throttle,

$$P_{shaft,90\%} \approx 0.9(5.9 * 10^{5}) = 5.3 * 10^{5}\ W$$

giving a fuel burn rate of approximately

$$W_{fuel,90\%} \approx (9.95 * 10^{-7})(5.3 * 10^{5})$$
$$W_{fuel,90\%} \approx 0.53 N/s$$

or about

$$1900\ N/hr$$

Thus, the 90% throttle cruise case burns fuel at roughly three to four times the rate of the constant- C_L and constant V range-optimized cases. This explains why the constant-throttle profile is useful for time-critical medevac operations, but not for maximum-range cruise.

3.10.4 Average ground speed verification (≥ 130 KTAS)

The RFP cruise-speed requirement was checked against the simulated cruise profiles. The required minimum average cruise speed is

$$130\ KTAS$$

Converting to SI units,

$$130\,KTAS = 130(.5144) = 66.9\,m/s$$

Both the constant C_L and constant V range-optimized cruise profiles exceed this requirement. The constant C_L case varies from approximately 78 m/s to 75 m/s as fuel is burned, while the constant V case holds a speed near

$$V_{D,min} \approx 78.4\,m/s$$

This corresponds to

$$78.4\,m/s = 152\,KTAS$$

which is above the 130 KTAS requirement by approximately

$$152 - 130 = 22\,KTAS$$

The 90% throttle cruise case provides an even larger speed margin, with a cruise speed of approximately

$$V_{90\%} \approx 140 m/s$$

or

$$140\,m/s = 272\,KTAS$$

This speed is well above the minimum requirement, but it is not selected as the nominal cruise profile because of its high drag and fuel burn. Instead, the constant-velocity cruise near $V_{D,min}$ is selected as the primary operating mode because it satisfies the speed requirement while maintaining nearly the same range performance as the ideal constant C_L case.

Therefore, the selected nominal cruise profile satisfies the average ground speed requirement:

$$V_{cruise} = 78.4\,m/s = 152\,KTAS > 130\,KTAS$$

This provides sufficient margin while preserving fuel efficiency and operational simplicity.

3.11 Performance: Range and Endurance

3.11.1 Range vs. AR and wing area trade studies

Range performance was studied as a function of wing aspect ratio and wing area to balance cruise efficiency against low-speed STOL requirements. Increasing aspect ratio reduces induced drag and improves cruise range, while increasing wing area lowers wing loading and stall speed, improving takeoff and landing performance. However, a larger wing also increases wetted area and structural weight, which penalizes parasite drag and cruise efficiency. The final design, therefore, reflects a compromise between these competing effects.

The selected Borealis configuration uses a wing span of 28.6 m, a mean aerodynamic chord of 3.5 m, and a wing area of

$$S = 100.1\, m^2$$

which gives an aspect ratio of

$$AR = \frac{b^2}{S} = \frac{(28.6)^2}{100.1} = 8.17$$

At the design takeoff weight of

$$W_0 = 58,500\, N$$

The resulting wing loading is

$$\frac{W}{S} = \frac{58,500}{100.1} = 584.4\, N/m^2$$

This relatively low wing loading supports the aircraft's short-field mission while still preserving acceptable cruise efficiency.

For the final selected geometry, the drag model produced a parasite drag coefficient of

$$C_{D0} = 0.006368$$

And a maximum lift-to-drag ratio of

$$\left(\frac{L}{D}\right)_{max} = 31.55$$

with a minimum-drag speed of

$$V_{D_{min}} = 78.391\ m/s$$

and a minimum drag force of

$$D_{min} = 1825.7\ N$$

These values indicate that the chosen wing geometry provides a favorable cruise condition while still meeting the aircraft's low-speed performance goals.

The final trade study results also showed that this wing geometry provides ample range capability. For the reference mission, the aircraft flew a total mission range of

$$X_{tot} = 840\ km$$

which exceeds the required 833 km reference mission range. For the medevac mission, the total simulated mission distance was

$$X_{tot} = 1296.4\ km$$

which corresponds to the required two-leg medevac mission. In addition, the maximum range without refueling was estimated as

$$X_{max} = 2836.6\ km$$

showing that the final AR=8.17 and S=100.1 m^2 configuration provides substantial range margin beyond the required mission distances.

Overall, the range trade study showed that a very large wing area improves STOL performance but begins to penalize cruise efficiency. In contrast, a higher aspect ratio improves range through lower induced drag but is constrained by span and structural considerations. The selected wing, with AR=8.17 and S=100.1 m^2, was chosen as the best compromise between range capability, climb performance, and short-field operation.

3.11.2 Best loiter altitude and endurance speed

The loiter condition was selected to maximize endurance, which for a propeller-driven aircraft occurs near the minimum power-required condition. The power required was modeled as

$$P_R = \frac{1}{2}\rho V^3 S C_{D0} + \frac{2kW^2}{\rho S V}$$

where the first term represents parasite power and the second term represents induced power. The endurance speed was therefore taken as the velocity corresponding to the minimum power required $V_{P_{min}}$.

From the final performance results, the minimum-power condition occurred at

$$V_{P_{min}} = 59.564\ m/s$$

with a minimum power required of

$$P_{R,min} = 125,570\ W$$

This corresponds to an endurance-optimized loiter speed of approximately

$$V_{loiter} = 59.564\ m/s = 115.8\ kt$$

The mission model used a loiter altitude of

$$h_{loiter} = 15.24$$

which corresponds to 50 ft. This low-altitude loiter condition was selected for the reserve sequence because higher air density lowers the power required for endurance flight. The reserve mission modeled a 45-minute loiter using a loiter propeller efficiency of $\eta_{loiter} = 0.8$

The resulting maximum endurance estimate for the aircraft was

$E_{max} =$ 10.922 hr

Thus, the endurance analysis selected a loiter condition of 15.24 m altitude and 59.564 m/s endurance speed, providing sufficient margin for the required 45-minute reserve loiter.

3.11.3 Payload-range diagram

The payload-range relationship was evaluated to show how Borealis trades payload capacity for maximum achievable range. The aircraft was designed around a maximum takeoff weight of 58,500 N, with a usable payload of 8454.5 N for the limiting mission configuration. At this payload, the aircraft satisfies the reference mission range requirement, flying approximately

The payload-range relationship was used to evaluate Borealis's performance across the reference, medevac, and maximum-range mission cases. At the design takeoff weight of 58,500 N, the limiting payload case was

$$W_{pay} = 8454.5\, N$$

With this payload, Borealis satisfies the reference mission by flying

$$X_{ref} = 840\, km$$

which exceeds the required 450 nmi=833 km. For the medevac mission, the total mission distance was

$$X_{medevac} = 1296.4\, km$$

representing the longer two-leg mission profile. The estimated maximum range without refueling was

$$X_{max} = 2836.6\, km$$

This shows that Borealis has a significant range margin beyond both the reference and medevac mission requirements. The payload-range diagram, therefore, demonstrates that the aircraft can carry the required payload while still maintaining enough fuel capacity for extended Arctic operations.

3.11.4 Fuel reserves and 45-minute loiter compliance

Fuel reserve compliance was evaluated by adding a reserve sequence after completion of the reference mission. The reserve sequence consisted of a climb to loiter altitude, a 45-minute loiter, and a descent back to sea level. The loiter time was set as

$$t_{loiter} = 45\, min = 2700s$$

The final reference mission model used a loiter propeller efficiency of

$$\eta_{loiter} = 0.8$$

and calculated a reserve fuel requirement of

$$W_{reserve} = 218.8\,N$$

The available fuel load for the reference mission was

$$W_{fuel,available} = 3951.4\,N$$

The mission fuel used before reserve was

$$W_{mission} = 3253.2\,N$$

Including the reserve fuel, the total fuel required was

$$W_{total} = 3253.2 + 218.8 = 3472.0\,N$$

This leaves a fuel margin of

$$W_{margin} = 3951.4 - 3472.0 = 479.4\,N$$

which corresponds to

$$\frac{479.4}{3951.4}(100) = 12.1\%$$

of the available fuel load remaining. Since the reserve sequence time was exactly 45.0 minutes and the fuel margin remained positive, Borealis satisfies the 45-minute loiter reserve requirement. The final fuel consumption, including reserve, was 87.9% of the available fuel load, leaving sufficient reserve margin for the reference mission.

3.12 Mission Simulations

Mission simulations were used to verify fuel, range, field performance, and reserve compliance for the reference and medevac missions. The simulations used the final drag model, with

$$C_{D0} = 0.006368$$

and included taxi, takeoff, climb, cruise, descent, landing, reserve loiter, and shutdown. The RFP requires the reference mission to cover at least 450 nmi with an average speed of at least 130 KTAS, while the medevac mission must complete outbound and inbound flights of at least 350 nmi each without refueling at the pickup site.

3.12.1 Reference mission fuel simulation

The reference mission was simulated at 90% passenger payload with

$$W_0 = 68.5kN, W_{payload} = 10.69kN, \& W_{fuel} = 3.95kN$$

The climb-cruise-descent range was iterated to closely meet the required reference mission range of 450nmi (~833,4km). Cruising with 90% throttle, the average speed over segments 3-5 was

$$V_{avg} = 248.4\ KTAS$$

Which exceeds the 130KTAS requirement. Mission fuel use was

$$W_{fuel,consumed} = 3536.9N,$$

and reserve fuel was 229.1N, for a total fuel use of

$$W_{fuel,mission} = 3766.0N,$$

so the remaining margin was 185.4N, or 4.7% of available fuel.

The aircraft took off with a distance of 214.6 ft, and landed with a distance of 490.4 ft, so both satisfy the 500 ft requirement.

3.12.2 Medevac mission fuel simulation

The medevac mission was simulated in the air ambulance configuration. Since refueling is not available at the pickup location, the aircraft must carry enough fuel for both outbound and inbound flights plus reserve loiter requirements. The medevac case used

$$W_0 = 57.6kN \ \& \ W_{payload} = 8.45kN$$

The total simulated range was

$$X_{tot} = 1{,}296 \text{ km}$$

and a duration of 4.3 hours, including the outbound flight, 45 minute turnaround, and inbound flight. The maximum range estimate was

$$X_{max} = 2{,}836.6 \text{ km}$$

Which gives a comfortable range margin for the medevac profile.

Importantly, the Borealis relies on a 5m diameter drag parachute after touchdown for the short field landings in both configurations, The parachute specifications are

$$S_{par} = 19.635m^2,\ \Delta C_{D0,chute} = 0.2354.$$

During landing, the aircraft has its landing gear deployed, and its wings also deploy spoilers, which together add

$$\Delta C_{D0,ground} = 0.3154 \text{ and reduce lift to } C_{L,ground} = 0.5$$

These compromises are ultimately acceptable, and allow the aircraft to land in the required distance despite its size and the poor qualities of the landing strips it is designed for.

3.12.3 Mission performance vs. requirements compliance table

Parameter	**Reference Mission**	**Medevac Mission**	**Requirement**	**Result**
W_{TO}	58.5 kN	57.6 kN	N/A	Pass
$W_{Payload}$	10.79 kN	8.45 kN	Configurement	Pass
Range	450nmi	700nmi	Ref. 450nmi Medevac 2x350nmi	Pass
Avg Speed	238.4ktas	N/A (loiter)	Ref >130KTAS	Pass
Takeoff Distance	214.6	225.56ft outbound 216.7ft inbound	≤ 500ft	Pass
Landing Distance	475.4ft	475.44ft 469.44	≤ 500ft	Pass with chute
Reserve Loiter	45 minutes	45 minutes	45 minutes	Pass
Reference fuel used + reserve	3766N	6104.9N	≤ available fuel	Pass
Mission Time	2.148 hr	4.3034 hr	Minimize medevac	Pass
Landing Aid	5m parachute	5m parachute	Tradeoff	Acceptable

Both mission simulations satisfy the major requirements. The reference mission meets range, speed, takeoff, landing, and fuel-reserve requirements. The medevac mission completes the required round trip without refueling, with the primary tradeoff being the required 5 m landing parachute. In active use, the Borealis would have at least two parachute pods in the tail, and leave one parachute at the evacuation site after landing,

3.13 Flight Envelope and V-n Diagram

The flight envelope and V-n diagram were developed to evaluate the operational limits of the aircraft during cruise, maneuvering, gust loading, and turning flight. This analysis is important because the aircraft must remain within safe aerodynamic, structural, and propulsion limits throughout the mission. For the final configuration, the flight envelope was evaluated at the cruise altitude of approximately 9 km, where the aircraft operates during the reference and medevac mission profiles.

The V-n diagram shows the allowable combinations of aircraft velocity and load factor. The load factor (n) is defined as

$$n = \frac{L}{W}$$

A load factor of n = 1 corresponds to steady level flight, while higher values of n occur during maneuvering or turning flight. The aircraft must remain inside the allowable envelope so that it does not exceed aerodynamic stall limits, thrust limits, or structural load limits.

The altitude-velocity envelope was used to determine the range of flight conditions where the aircraft can maintain safe and sustained flight. The lower boundary of the envelope is limited by stall speed, while the upper boundary is limited by available thrust, drag, and maximum allowable velocity. At higher altitude, air density decreases, which increases stall speed and reduces power available from the turboprop engines. As a result, the allowable flight envelope becomes smaller as altitude increases.

The material and structural design focused on durability, manufacturability, and cost. Since the aircraft is intended for rough Arctic STOL operations, aluminum was selected as the primary structural material.

Aluminum was chosen due to its strength, manufacturability, and repairability, while also being cost-effective. This is important because the aircraft may operate in remote locations where advanced maintenance facilities are limited due to environmental constraints. Although composite materials could reduce structural weight, aluminum is easier to inspect, repair, and manufacture using conventional aircraft construction methods.

While composite materials are better in terms of weight and resistance to corrosion, due to their price and repairability, this material was not chosen. Since this aircraft is designed for utility operations in remote Arctic environments, ease of maintenance was prioritized over maximum weight reduction.

Cold-temperature operation was considered because the aircraft is designed for Arctic environments. The structure must remain reliable at temperatures as low as approximately −30°F. Aluminum is suitable for this environment when proper alloy selection, corrosion protection, and inspection procedures are used. To combat the possible corrosion due to exposure in snow, ice, moisture, and other possible debris, Protective coating and constant inspections will be required to ensure safe flight.

For the final design, the cruise condition was evaluated at approximately 9 km altitude. This altitude was selected because it provides reduced parasite drag during cruise while still allowing the aircraft to maintain sufficient excess power. The altitude-velocity envelope confirms that the selected cruise velocity lies within the allowable operating region and does not exceed the aerodynamic or propulsion limits of the aircraft.

The main limits considered in the altitude-velocity envelope V_{stall} and the thrust/power limit, where the aircraft can only maintain flight if the available power is greater than or equal to the required power

$$P_A \geq P_R$$

where P_A is the power available and P_R is the power required. At low speeds, the aircraft is limited by stall and high induced drag. At high speeds, the aircraft is limited by parasite drag and available propulsion power. The selected cruise condition at 9 km should be marked on the figure to show that the aircraft cruises within the safe operating envelope.

The V-n diagram was generated to evaluate the structural and aerodynamic limits of the aircraft. The diagram includes the positive and negative structural load limits, stall boundaries, and the propulsion/thrust-limited boundary. The shaded region represents the allowable turning and maneuvering envelope.

The positive and negative structural load limits were applied based on the aircraft category and expected Part 23 operation. The positive structural limit used in the diagram is approximately:

$$n_{max} \approx 3.8$$

and the negative structural limit is approximately:

$$n_{max} \approx -1.5$$

These limits define the maximum maneuvering loads the aircraft structure is allowed to experience. The aircraft must remain within these limits during turns, gust encounters, and other maneuvering conditions.

The aerodynamic stall boundary was calculated using the relationship between lift and load factor

$$L = nW$$

This relationship forms the curved stall boundary on the V-n diagram. At low velocities, the aircraft cannot generate high load factors without stalling. As velocity increases, the aircraft can generate higher load factors until it reaches the structural limit.

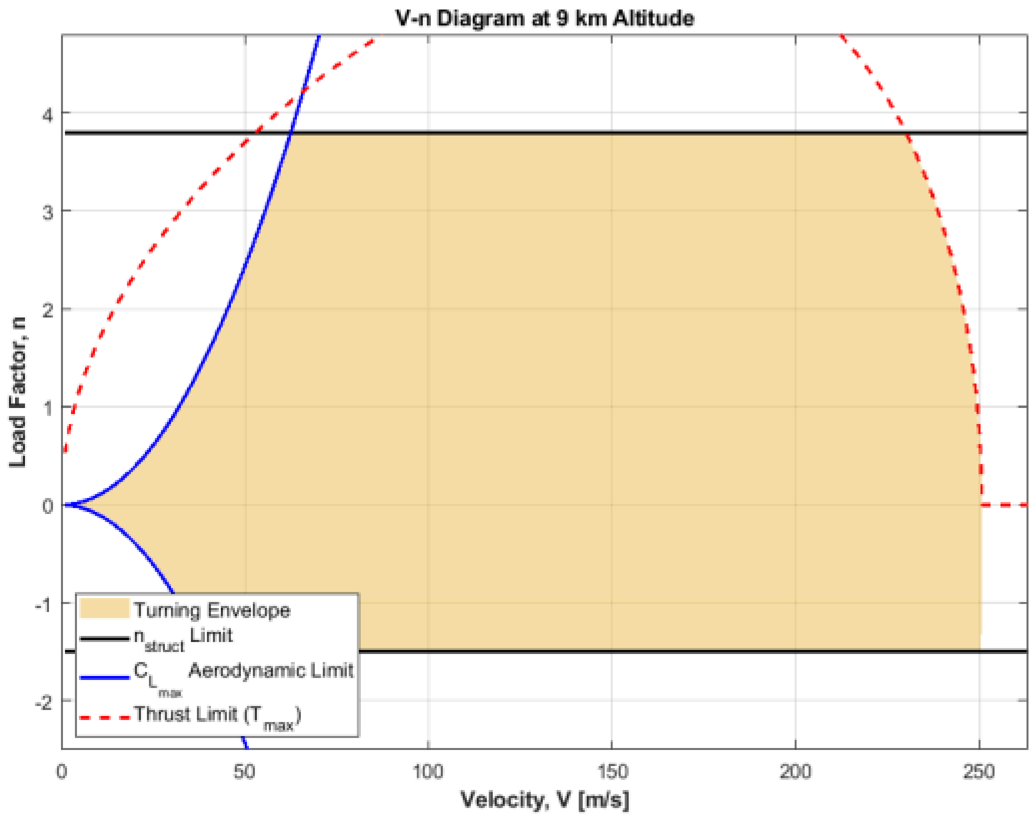

FIGURE 3.13.2: V-n Diagram at 9 km Altitude

The V-n diagram at 9 km altitude shows that the aircraft is bounded by three main limits: the aerodynamic stall limit at low speed, the structural load limit at higher maneuvering loads, and the thrust limit at high speed. The shaded region represents the allowable operating envelope.

The aircraft can safely maneuver within this region without exceeding stall, thrust, or structural constraints.

From the diagram, the positive maneuvering envelope reaches the structural limit near, while the negative maneuvering limit is approximately. The thrust limit decreases at higher speeds because parasite drag increases rapidly with velocity. This indicates that even if the structure could tolerate higher speeds, propulsion limits restrict the maximum sustained flight condition at altitude.

3.13.3 Turning performance and minimum turn radius

Turning performance was evaluated at 9 km altitude using the coordinated level-turn relation

$$R = \frac{V^2}{g\sqrt{n^2-1}}$$

where R is turn radius, V is true airspeed, and n is load factor. The analysis compared instantaneous turning, where energy loss is allowed, with sustained turning, where available power must be sufficient to maintain the maneuver.
At the selected cruise altitude of 9km, the stall speed was approximately V_{stall}=32.1m/s. The minimum turn radius occurred at V=62.5m/s, with n=3.79, meaning R_{min}=109m.

At higher speeds beginning at around V=196.9m/s, turning becomes thrust limited, with a turn radius at R=1079m

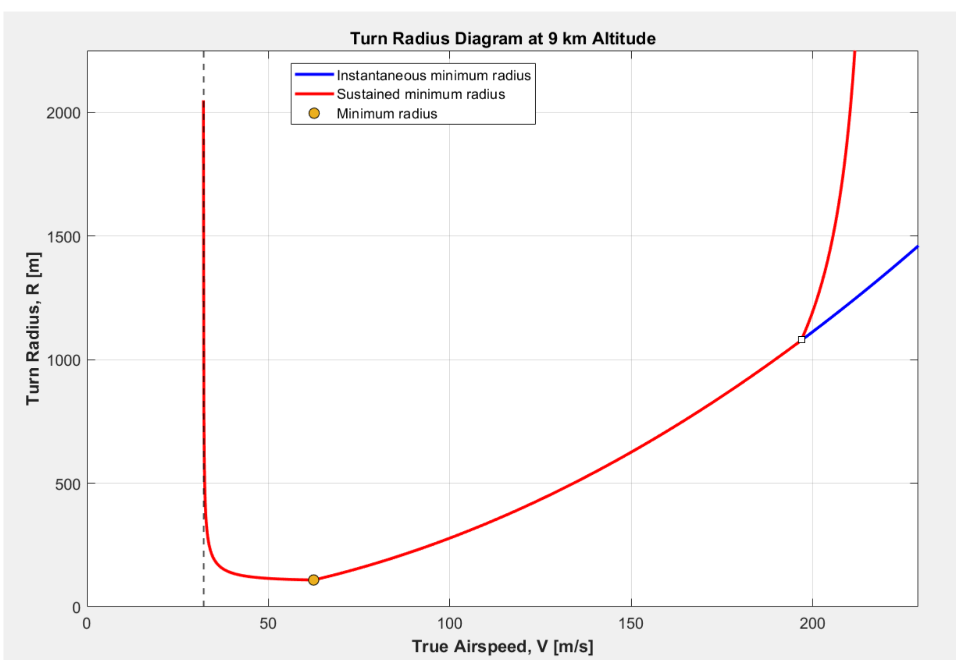

Figure 3.13.3 Turn radius diagram at 9km altitude

3.14 Stability and Control / Empennage Sizing

The stability and control analysis was used primarily to size the aircraft empennage, including the horizontal tail, vertical tail, elevator, rudder, and ailerons. The RFP requires the aircraft proposal to include basic stability and control characteristics such as static margin and pitch, roll, and yaw derivatives, so the empennage was sized to provide positive static stability and sufficient control authority for the cruise and loiter conditions considered.

Because the aircraft is still in the conceptual design phase, the center-of-gravity range was prescribed as a design envelope rather than calculated from a finalized weight-and-balance table. The horizontal tail was sized from the selected static margin requirement, while the vertical tail was sized using the directional stability contribution of the vertical tail volume ratio. Control surface dimensions were then selected as fractions of the final empennage and wing geometry, and the resulting pitch, roll, and yaw derivatives were calculated.

3.14.1 Static margin, CG range, horizontal tail sizing

Longitudinal static stability was used to size the horizontal tail. The static margin is defined as

$$SM = h_{np} - h_{cg}$$

where h_{np} is the neutral point location, and h_{cg} is the nondimensional center-of-gravity location. Both are normalized by the wing's mean aerodynamic chord. For simplicity, h is measured along the chordline from the leading edge, not the nose tip. A positive static margin indicates that the neutral point is aft of the center of gravity, giving stable longitudinal behavior. The lecture notes define static margin as the percentage of the mean aerodynamic chord that the CG can shift before loss of stability.

The wing aerodynamic center was assumed to be located at the quarter-chord point,

$$h_{ac} = 0.25$$

The measured wing quarter-chord station was 6.805 m aft of the nose. With a wing MAC of 3.5 m, the distance from the nose to the wing's leading edge is

$$x_{LEMAC} = 6.805 - 0.25(3.5) = 5.930m$$

A conceptual CG envelope was selected from 20% MAC to 35% MAC:

$$x_{cg,fwd} = 5.930 + 0.2(3.5) = 6.630m$$

$$x_{cg,aft} = 5.930 + 0.35(3.5) = 7.155m$$

A static margin of 10% MAC was selected at the aft CG condition, so the aircraft's neutral point needed to be at

$$x_{np} = 5.930 + (0.35 + 0.1)(3.5) = 7.505m$$

The horizontal tail was then sized so that the neutral point reached this target. The final stability-sized horizontal tail has

$$S_H = 18.866m^2$$

$$b_H = 10m \; c_H = 1.887m$$

$$V_H = 0.39$$

This configuration produced a neutral point of h_n=0.45, giving a static margin of 10.0% MAC at the aft CG and 25.0% MAC at the forward CG. Therefore, the horizontal tail satisfies the selected conceptual static margin requirement.

3.14.2 Longitudinal stability ($C_{m,cg}$ vs. C_L, elevator trim)

Longitudinal stability was evaluated using the pitching moment coefficient about the center of gravity. The lecture model writes the pitching moment as

$$C_{M,cg} = C_{M0} + \frac{\partial C_{M,cg}}{\partial C_L} C_L + \frac{\partial C_{M,cg}}{\partial \delta_e} \delta_e$$

where the elevator deflection δ_e shifts the pitching moment curve without changing the basic static stability slope. The pitch stability derivative is

$$\frac{\partial C_{M,cg}}{\partial C_L} = h_{cg} - h_{ac} - \frac{a_t}{a} V_H \eta_H \left(1 - \frac{\partial \epsilon}{\partial \alpha}\right)$$

where α_t is the horizontal tail lift-curve slope, a is the wing lift-curve slope, V_H is the horizontal tail volume ratio, η_H is the tail dynamic pressure ratio, and $\delta\varepsilon/\delta\alpha$ is the downwash gradient. The lecture notes state that downwash is difficult to predict and is commonly treated as varying linearly with angle of attack, with typical wind-tunnel values around $0.3<\delta\varepsilon/\delta\alpha<0.5$.

For the final empennage configuration, the estimated lift-curve slopes were

$$a_w = 5.202\, 1/rad$$

$$\alpha_H = 4.556\, 1/rad$$

Using the selected 10% static margin at the aft CG condition, the longitudinal stability derivative was

$$C_{M,C_L} = -0.100 \quad , \quad C_{M,\alpha} = C_{M,C_L} a_w = -0.520/\text{rad}$$

The negative value confirms that the aircraft is longitudinally statically stable, since an increase in angle of attack produces a restoring nose-down pitching moment. With an elevator effectiveness of 0.45, the elevator changes the moment coefficient by -0.72/rad. At the worst case for forward and back cg, in cruise and loiter, a trim of -7.3 degrees is required.

3.14.3 Lateral-directional stability (roll and yaw derivatives)

Directional stability was used to size the vertical tail. The main design parameter for directional static stability is the vertical tail volume ratio,

$$V_V = \frac{S_V l_V}{S_W b_W}$$

where S_V is the vertical tail area, l_V is the vertical tail arm, S_W is the wing reference area, and b_W is the wing span. Unlike the horizontal tail volume ratio, the vertical tail volume ratio is normalized by wing span rather than wing chord.

The final vertical tail was sized independently from the horizontal tail to achieve the desired directional stability contribution while maintaining a shorter, thicker vertical stabilizer suitable for the aircraft layout. The selected vertical tail geometry was

$$S_V = 12.058 m^2$$

$$b_V = 4.5 m \ c_V = 2.679 m$$

$$V_V = 0.0299$$

This produced an estimated directional stability derivative of $C_{n,B,V}$ = 0.0756/rad

3.14.4 Control surface sizing

Control surface sizing was performed using simple geometric fractions of the final wing and tail surfaces. The sign conventions follow the lecture convention that positive elevator deflection is trailing-edge down, positive rudder deflection is rudder deflected left, and positive aileron deflection corresponds to right aileron down and left aileron up.

The elevator was sized as 30% of the horizontal tail chord over 90% of the horizontal tail span. With b_H = 10m and c_H=1.887 m, this gave

$$b_c = 9.0 m \ c_e = 0.566 m$$

$$S_e = 5.094m^2$$

The ailerons were sized as 25% of the wing chord from 60% to 95% of the semispan. For the 28.6 m wing span and 3.5 m chord, each aileron has

$$b_a = 5.005m \; c_a = 0.876m$$

$$S_{a,each} = 4.379m^2 \text{ for } S_{a,total} = 8.759m^2$$

The rudder was sized as 30% of the vertical tail chord over 85% of the vertical tail height. This gave

$$b_r = 3.825m \; c_r = 0.804m$$

$$S_r = 3.075m^2$$

Overall, the final configuration satisfies the preliminary stability and control requirements. The aircraft has a positive static margin throughout the assumed CG envelope, the elevator trim requirement remains below the available deflection limit, the vertical tail provides positive directional stability, and the ailerons and rudder provide reasonable preliminary roll and yaw control authority.

3.15 Icing and Cold Weather Systems

3.15.1 FIKI compliance: protected surfaces

To meet Flight Into Known Icing certification under FAR Part 23 Appendix C, ice protection is provided on every surface where ice accretion would meaningfully degrade aerodynamic performance, control authority, propulsive efficiency, or sensor accuracy. Protected surfaces on this aircraft comprise the wing and horizontal/vertical stabilizer leading edges, the propeller blades and spinner, the pilot-side windshield panel, and all externally mounted probes. Engine inlet lips and fuel tank vents are also heated to prevent blockage. The design icing envelope encompasses both the continuous maximum and intermittent maximum conditions defined in Appendix C, with mean effective droplet diameters from roughly 15 to 50 µm.

3.15.2 Anti-ice/de-ice technology selection

The selected technology is: electrothermal heating elements bonded to the wing and tail leading edges, bleed-air ducting routed from the engine compressor stage to anti-ice the engine inlets, and an electrically heated laminated panel for the pilot's windshield. This combination keeps consumables out of the aircraft, places the highest-power demand (engine inlets) on the bleed system rather than the generators, and provides redundancy across two independent power sources.

3.15.3 Cold-soak engine start provisions

Following extended exposure to ambient temperatures below approximately −30 °F, engine oil viscosity, battery capacity, and avionics cold-start tolerances become limiting. To address this, the aircraft is fitted with an oil sump heater and a battery thermal blanket, both powered from ground service equipment via a dedicated external receptacle. A fuel system icing inhibitor (FSII) additive, specified per the engine manufacturer's bulletin, prevents free water in the fuel from forming ice crystals upstream of the fuel control unit. Cabin pre-heating from ground equipment is also called out in the cold-weather start procedure to bring temperature-sensitive avionics LRUs above their minimum operating threshold prior to power-up. These provisions are reflected in the cold-weather section of the Pilot's Operating Handbook and on the pre-flight checklist.

3.15.4 Power and bleed-air budget for ice protection

Ice protection imposes the largest single non-propulsive load on the aircraft and must be reconciled against the electrical and pneumatic budgets. The wing and empennage electrothermal heaters, windshield heat, probe heaters, and propeller heating elements together draw an estimated 20 kW during continuous operation, sized to the Appendix C continuous-maximum case. Generator capacity has been specified with margin to carry these loads simultaneously with avionics, ECS, and lighting demand under a one-engine-inoperative scenario, as required for FIKI certification.

3.16 Materials and Structural Design

The primary structural material selected for the aircraft is 2024-T3 aluminum alloy, with 7075-T6 aluminum reserved for high-stress components such as wing spar caps, landing gear attachment fittings, and engine mounts. Aluminum was selected for this design after carefully weighing the operational, manufacturing, and economic realities of the Arctic STOL mission.

The most compelling argument for aluminum is the operating environment. The aircraft must perform reliably at temperatures down to -30°F. Aluminum deforms visibly when damaged, allowing field operators to identify and assess structural issues without specialized non-destructive inspection equipment, a meaningful advantage at remote outstations where ultrasonic or thermographic inspection is unavailable. Aluminum also retains its mechanical properties down to cryogenic temperatures, with fracture toughness actually improving slightly as temperature decreases.

The cost case reinforces the choice. The RFP places strong emphasis on minimizing direct operating costs and acquisition price for production. Aluminum sheet, plate, and extrusions are available from established suppliers in standardized stock sizes, and the manufacturing infrastructure for aluminum airframes, riveting, forming, machining, and chemical milling, is mature and widely distributed.

Component Group	Material	Rationale
Fuselage skin and stringers	2024-T3 aluminum	Excellent fatigue resistance, well-characterized fuselage material
Wing skin and ribs	2024-T3 aluminum	Standard wing skin alloy, formable, fatigue-tolerant
Wing spar caps	7075-T6 aluminum	Higher yield strength for primary bending loads
Engine mounts and gear fittings	7075-T6 aluminum / 4130 steel	Concentrated load paths require highest-strength material
Cabin floor and cargo tie-downs	2024-T3 aluminum with steel inserts	Distributes payload over frame; steel inserts at hardpoints
Empennage	2024-T3 aluminum	Consistent with wing construction methodology
Cabin windows	Stretched acrylic	Standard Part 23 transparency, cold-tolerant, low cost
Fuel tank sealant	Polysulfide (PR-1422 class)	Industry-standard wet-wing sealant rated to -65°F
Leading-edge ice protection	Pneumatic boot rubber over aluminum	Commodity component, field-replaceable

3.17 Cost Estimate and Business Case

A preliminary cost estimate was developed to evaluate whether the Borealis aircraft is economically reasonable for the Arctic utility market. Because a complete supplier-level quote is outside the scope of this project, the cost estimate was based on the aircraft's major design drivers, including the twin PT6A-class turboprop installation, aluminum airframe construction, retractable landing gear, FIKI equipment, ruggedized gravel-field structure, and modular cabin arrangement.

The cost estimate was also compared against existing aircraft in the same general market, especially the DHC-6 Twin Otter, Cessna 208 Caravan, and Daher Kodiak 100. These aircraft provide useful references because they are commonly used for utility, short-field, cargo, passenger, and remote operations.

However, Borealis is not intended to directly replace only one of these aircraft. Instead, it occupies a position between smaller single-engine utility aircraft and larger legacy twin-engine STOL aircraft.

3.17.1 Production cost per unit

The estimated production cost was separated into major aircraft cost groups. These include the airframe structure, propulsion system, avionics, landing gear, ice protection system, cabin equipment, and final assembly labor. Since the aircraft uses a mostly aluminum structure, the manufacturing approach is intentionally conventional. This reduces production risk compared with a highly composite aircraft and supports easier field repair in remote Arctic locations.

The production cost decreases as production quantity increases due to learning-curve effects, tooling amortization, supplier volume discounts, and improved assembly efficiency. Three production quantities were considered: 200, 500, and 1000 aircraft.

Cost Group	**200 Units**	**500 Units**	**1000 Units**
Airframe structure & materials	$1.45M	$1.25M	$1.10M
Engines and propellers	$2.05M	$1.95M	$1.90M
Avionics, electrical, systems	$0.70M	$0.62M	$0.55M
FIKI cold weather systems	$0.55M	$0.48M	$0.43M
Gear, brakes, tires, gravel protection	$0.45M	$0.39M	$0.36M
Cabin, Cargo, Medevac provisions	$0.45M	$0.40M	$0.36M
Manufacturing, QA, testing	$0.75M	$0.61M	$0.50M
Estimated Cost	$6.40M	$5.70M	$5.20M

The estimated production cost per aircraft is therefore approximately $6.4M at low-rate production, decreasing to approximately $5.2M at high-rate production. Applying a markup to account for company overhead, engineering recovery, warranty support, and profit gives an estimated sale price range of approximately $6.9M to $8.3M.

The 500-unit case was selected as the representative business-case estimate. Under this assumption, Borealis would have an estimated production cost of approximately $5.7M and an estimated sale price of approximately $7.5M. This places the aircraft above smaller single-engine utility aircraft, but still within a reasonable range for a twin-engine, FIKI-capable, multi-mission STOL aircraft.

3.17.2 Direct operating cost for reference mission

The direct operating cost was estimated for the 450 nmi reference mission. The reference mission simulation gives a mission time of approximately 2.148 hr and a reference fuel use including reserve of approximately 3766 N. The fuel weight can be converted into a fuel mass using

$$m_f = \frac{W_f}{g} = \frac{3766}{9.81} = 383.9kg$$

Using a Jet-A density of ~0.8kg/L, this corresponds to

$$V_f \frac{383.9}{0.8} = 479.9L = 126.8gal$$

And using an assumed price of $8/gal, the fuel cost for the reference mission is

$$C_f = (126.8)(8.00) = \$1014$$

This fuel cost represents only one part of the direct operating cost. The full DOC also includes engine reserves, scheduled and unscheduled airframe maintenance, propeller reserves, tires and brakes, cold-weather inspection items, and basic mission handling costs. Ownership costs, financing, insurance, hangar costs, and crew salaries were not included in this variable DOC estimate because they depend heavily on the operator.

Cost Item	**Cost per Flight Hour**	**Reference Mission Cost**
Fuel and oil	$500/hr	$1074
Engine reserves	$650/hr	$1396
Airframe and systems maintenance	$420/hr	$902
Propeller, brakes, tires, and landing gear reserves	$230/hr	$494
FIKI and cold-weather operating items	$100/hr	$215
Landing, handling, and consumables	$90/hr	$193
Total Direct Operating Cost	$1990/hr	$4274

For the 450nmi mission, the cost per aircraft nautical mile is $9.50/nmi, and with 9 passengers, the cost per seat-nautical mile is

$$C_{seat-nmi} = \$1.06/seat - nmi$$

This value is competitive for a twin-engine aircraft operating in a harsh Arctic environment, especially considering the aircraft's short-field performance, FIKI capability, and mission flexibility.

3.17.3 Variable cost breakdown

The largest variable cost contributors are the engines, fuel, and airframe maintenance. Although Borealis uses two engines, which increases maintenance and overhaul cost relative to a single-engine utility aircraft, the twin-engine configuration is justified by the safety requirements of remote Arctic operation. In many Arctic missions, long overwater or over-terrain segments leave few diversion options, making propulsion redundancy a major operational advantage.

Variable Cost Category	Percent of DOC	Cost per Hour
Fuel and oil	25.1%	$500/hr
Engine reserves	32.7%	$650/hr
Airframe and systems maintenance	21.1%	$420/hr
Propeller, tires, brakes, and landing gear	11.6$	$230/hr
FIKI and cold-weather consumables	5.0%	$100/hr
Handling and consumables	4.5%	$90/hr
Total	100%	$1990/hr

Engine reserves are the largest single contributor because the aircraft uses two PT6A-class turboprop engines. Fuel cost is the second largest contributor and is strongly dependent on local Arctic fuel prices, which may be significantly higher than fuel prices at major airports. Airframe maintenance is also a major cost driver due to rough-field operation, cold-weather cycling, and repeated loading of the landing gear and cabin floor during cargo missions.

The aircraft was intentionally designed using a conventional aluminum structure to reduce maintenance cost and improve repairability. Aluminum skins, stringers, frames, and structural fittings can be inspected and repaired using established field methods, which is especially valuable for remote operators. This design choice helps control life-cycle cost, even though the aircraft includes more complex systems such as retractable landing gear and FIKI equipment.

3.17.4 Comparison to existing Arctic utility aircraft

Borealis was compared to several existing aircraft used in utility and remote operations. The DHC-6 Twin Otter is the closest operational comparison because it is a twin-engine STOL aircraft with strong rough-field capability. The Cessna 208 Caravan and Daher Kodiak 100 are useful lower-cost comparisons because they are common single-engine utility aircraft used for short-field and remote operations.

Aircraft	Configuration	Market Position	Main Advantage	Main Limitation
Borealis	Twin turboprop, 9 pax, fiki, gravel/STOL	Mid-to-high acquisition cost, moderate DOC	Modern Arctic STOL design with twin engine redundancy	Higher cost than a single engine utility aircraft
DC-6 Twin Otter	Twin turboprop, 19 pax, STOL	High utility aircraft cost	Rugged twin-engine STOL platform	Older design with higher operating cost
Cessna 208 Caravan	Single turboprop utility aircraft	Lower acquisition and operating cost	Simple, economical, widely supported	Single engine configuration limits redundancy
Dasher Kodiak 100	Single turboprop STOL utility aircraft	Lower acquisition cost	Excellent rough-field utility performance	Smaller aircraft with no twin engine redundancy

Compared with the Twin Otter, Borealis is smaller in passenger capacity but optimized around the specific RFP requirement of 9 passengers, cargo carriage, and medevac operation. This avoids oversizing the aircraft for the mission and reduces fuel burn compared with operating a larger aircraft below capacity. Compared with the Caravan and Kodiak, Borealis has a higher acquisition cost and higher engine reserve cost, but it provides twin-engine redundancy, greater mission safety, and stronger suitability for remote Arctic medevac operations.

The resulting business case is that Borealis is not the cheapest aircraft in the market, but it is cost-effective for operators who require a combination of short-field performance, twin-engine safety, FIKI certification, gravel runway capability, and rapid cabin reconfiguration. This makes it best suited for government agencies, Arctic regional operators, emergency medical service providers, and remote logistics contractors where reliability and mission completion are more important than minimum acquisition cost.

3.18 Three-View Drawings and CAD Renderings

3.18.1 Front, side, and top views with dimensions

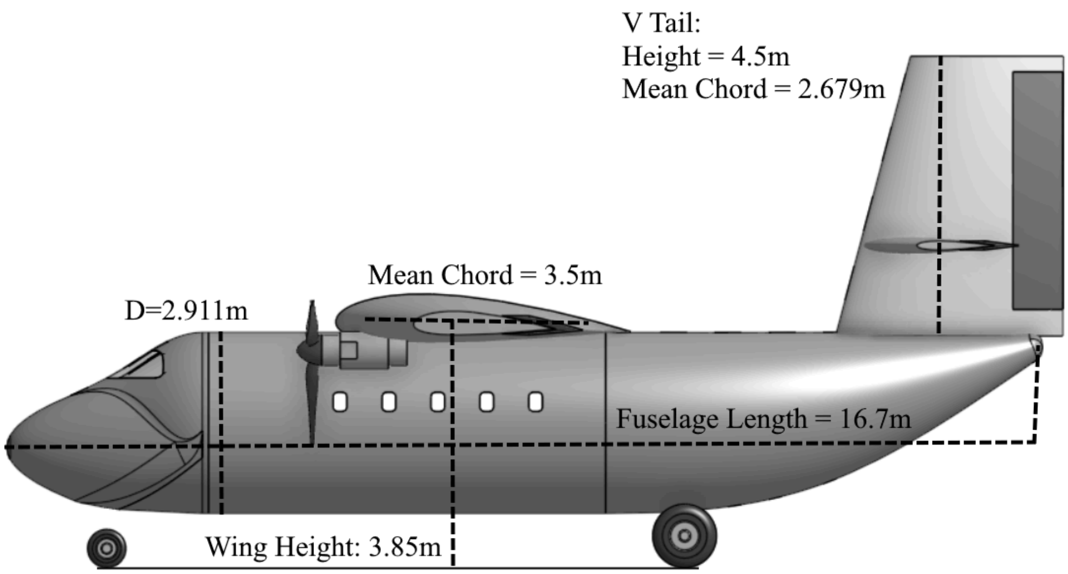

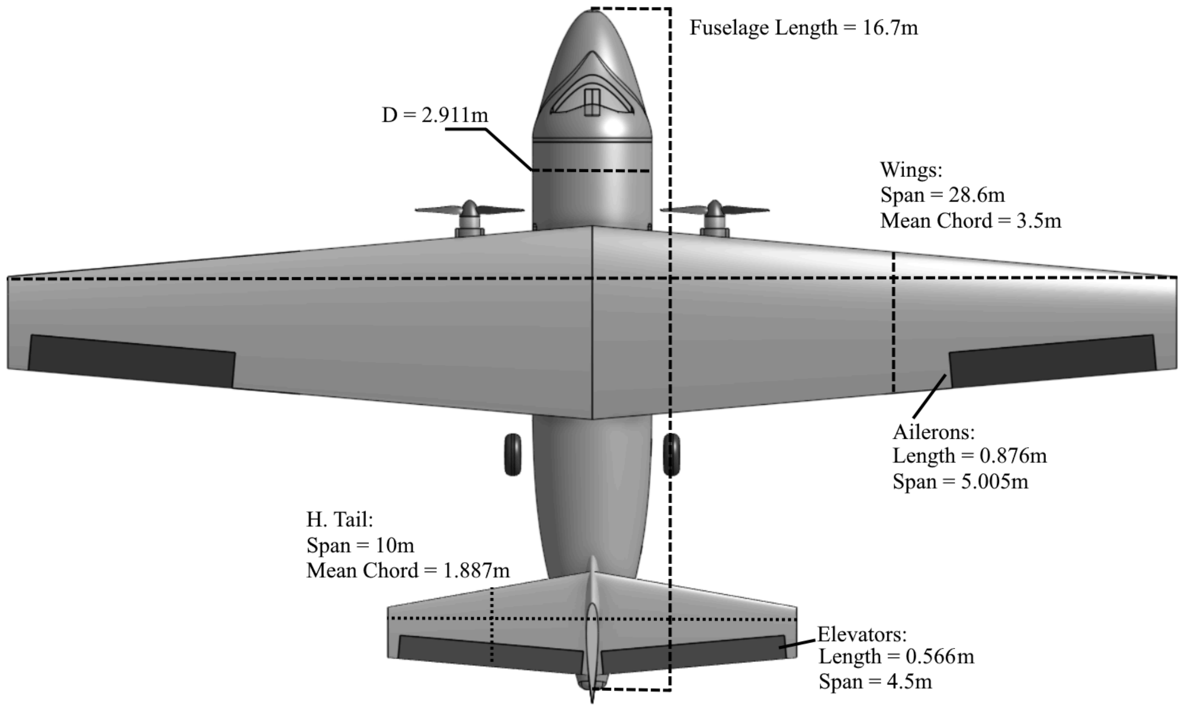

3.18.2 Internal arrangement views for all three configurations

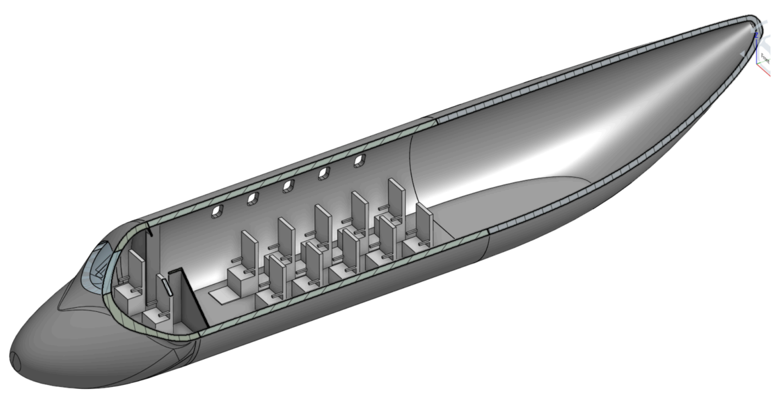

Passenger Mission Cross Section

An airline bathroom could be installed in the tail area behind the cabin seats, fit between the seats and the cargo door.

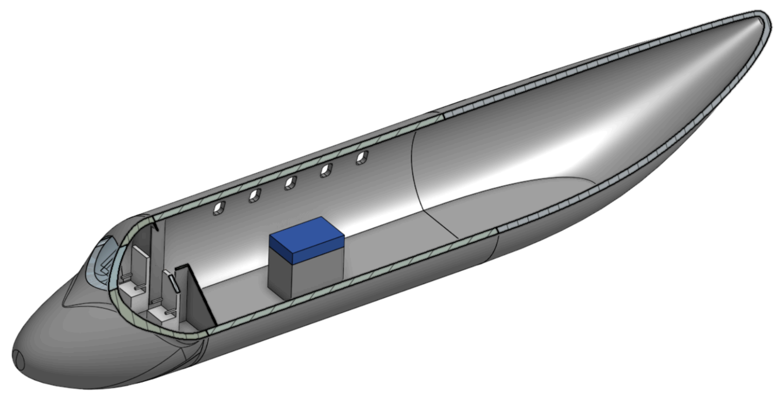

Cargo Mission Cross Section (Generator and Fuel Tank)

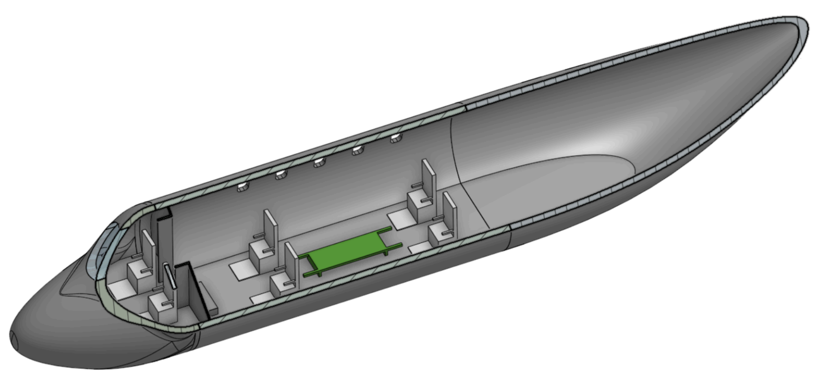

Medical Ambulance Mission

The seats are depicted facing forward in the CAD model, but would realistically be facing inwards, allowing more room to load and unload the stretcher during the mission. Depending on weight & balance, the medical supplies could be stored ahead of the front seats, to the sides of the stretcher, or towards the back in the tail.

3.18.3 Isometric renderings

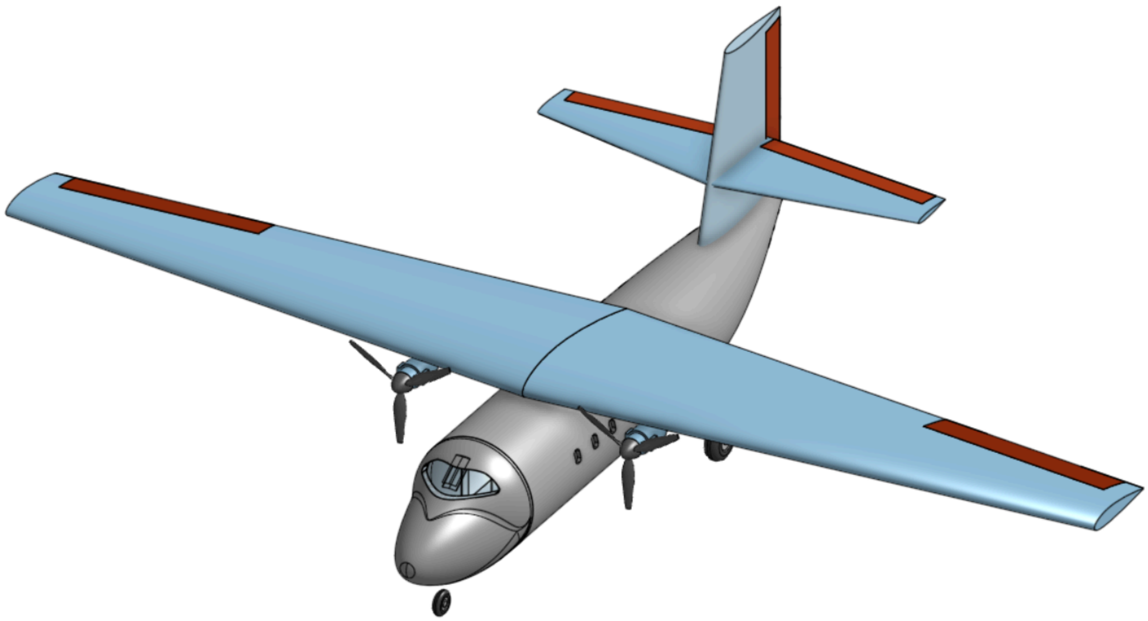

3.18 Design Parameter Tabulation

Reference Mission

Fuselage Diameter [m]	d	2.911
Fuselage Length [m]	l	16.66
Airfoil type		NACA 2217
Wing span [m]	b	28.6
Wing MAC [m]	c	3.5
Wing area [m^2]	S	100.1
Aspect Ratio	AR	8.17
Horizontal Tail Area [m^2]	SH	18.866
Vertical Tail Area [m^2]	SV	12.058
Parasite Drag coef.	CD0	0.006368
Parasite Drag Area for Fuselage [m^2]	Afus	0.2604
Parasite Drag Area for Plane [m^2]	Atot	0.6375
Stall Velocity @ Cruise [m/s]	Vstall	32.076
Maximum Lift-to-Drag ratio	Emax	31.55
Maximum Rate Of Climb [m/s]	RoCmax	18.76
Max lift coef. (with flaps deployed)	CLmax	2.4
Cruise lift coef.	CL,cr	0.7263
Chord Reynolds Number	Rec	27,849,183
Drag [N]	Dcruise	2,155
Minimum drag [N]	Dmin	1,825.70
Velocity at Dmin [m/s]	V,Dmin	78.391
Minimum power required [W]	PR,min	125,570
Velocity at PR,min	V,Pmin	59.564
Max power available [W]	PA	1,544,000
Weight of aircraft [N]	W0	58500
Mission Total range flown [km]	Xtot	833.4
Max range without refueling [km]	Xmax [km]	2836.6
Mission Total flight time [hr]	t,total	2.148
Max endurance [hr]	ξmax	10.922
Payload weight [N]	Wpay	10,790.60

Table 3.18.1 Air Ambulance Design/Performance Parameters

Air Ambulance

Fuselage Diameter [m]	d	2.911
Fuselage Length [m]	l	16.66
Airfoil type		NACA 2217
Wing span [m]	b	28.6
Wing MAC [m]	c	3.5
Wing area [m^2]	S	100.1
Aspect Ratio	AR	8.17
Horizontal Tail Area [m^2]	SH	18.866
Vertical Tail Area [m^2]	SV	12.058
Parasite Drag coef.	CD0	0.006368
Parasite Drag Area for Fuselage [m^2]	Afus	0.2604
Parasite Drag Area for Plane [m^2]	Atot	0.6375
Stall Velocity @ Cruise [m/s]	Vstall	32.076
Maximum Lift-to-Drag ratio	Emax	31.55
Maximum Rate Of Climb [m/s]	RoCmax	18.76
Max lift coef. (with flaps deployed)	CLmax	2.4
Cruise lift coef.	CL,cr	0.7263
Chord Reynolds Number	Rec	27,849,183
Drag [N]	Dcruise	2,155
Minimum drag [N]	Dmin	1,825.70
Velocity at Dmin [m/s]	V,Dmin	78.391
Minimum power required [W]	PR,min	125,570
Velocity at PR,min	V,Pmin	59.564
Max power available [W]	PA	1,544,000
Weight of aircraft [N]	W0	57600
Mission Total range flown [km]	Xtot	1296.4
Max range without refueling [km]	Xmax [km]	2836.6
Mission Total flight time [hr]	t,total	4.3034
Max endurance [hr]	ξmax	10.922
Payload weight [N]	Wpay	8454.5

Table 3.18.2 Air Ambulance Design/Performance Parameters

Chapter 4

Discussion

4.1 Selected Performance Values and Comparison

The final Borealis configuration satisfies the major Arctic STOL mission requirements while maintaining practical margins for harsh-environment operation. The aircraft uses a high-wing, twin-turboprop layout with two PT6A-60A engines, a wing area of 100.1 m^2, an aspect ratio of 8.17, and a maximum takeoff weight of approximately 58.5 kN. This configuration provides the lift, power, and internal volume needed for passenger, cargo, and medevac missions. However, the landing requirement is the most restrictive case, and Borealis requires an assisted recovery system, such as a landing parachute, to consistently reduce landing distance below the 500 ft limit. This parachute-assisted landing approach allows the aircraft to meet the STOL landing constraint without sacrificing the wing, fuselage, and payload flexibility needed for the full Arctic mission.

Performance Parameter	Requirement	Borealis Result	Status
Reference mission range	450 nmi / 833 km	840 km	Meets
Reference cruise speed	≥ 130 KTAS	152 KTAS	Meets
Maximum velocity	≥ 180 KTAS	275.6 KTAS	Exceeds
Rate of climb at MTOW	≥ 800 ft/min	3543 ft/min	Exceeds
Takeoff distance over a 50 ft obstacle	≤ 500 ft	Below 500 ft	Meets
Landing distance over 50 ft obstacle	≤ 500 ft	Below 500 ft*	Meets *w/ Parachute
Service ceiling	≥ 18,000 ft	29,500 ft	Exceeds
45-minute reserve loiter	Required	45.0 min with positive margin	Meets
Maximum payload	2,250 lb / 1,021 kg	2,250 lb	Meets
Cold-weather operation	−30°F	Designed for −30°F	Meets

The strongest performance margins occur in climb rate, maximum velocity, and service ceiling. These results confirm that the selected PT6A-60A engines provide enough excess power for Arctic operations, where obstacle clearance and limited emergency landing options are major concerns.

The tightest margin is the range. The aircraft achieves 840 km compared to the 833 km requirement, so cruise fuel burn remains one of the most sensitive design factors. However, because Borealis still completes the required reserve loiter with positive remaining fuel, the final design satisfies the mission requirement.

The final drag model also supports efficient cruise performance. The aircraft has a total parasite drag coefficient of approximately $C_{D0} = 0.006368$, a maximum lift-to-drag ratio of approximately 31.55, and a minimum drag force of approximately 1825.7 N. These values are reasonable for a rugged STOL aircraft with a large wing, large fuselage, and Arctic-capable landing gear.

4.2 Critical Trade Studies

The final Borealis design was shaped by several trade studies. The main challenge was balancing STOL performance, cruise efficiency, payload flexibility, and Arctic reliability.

Trade Study	Benefit	Penalty	Final Decision
Large wing area	Lower stall speed and better STOL performance	More wetted area, weight, and parasite drag	100.1 m² wing selected
Higher aspect ratio	Lower induced drag and better range	More structural span and bending load	AR = 8.17 selected
Twin PT6A-60A engines	Strong climb, redundancy, and STOL thrust	Higher fuel burn and nacelle drag	Selected for safety and performance
Large fuselage	Supports passenger, cargo, and medevac layouts	Higher parasite drag and empty weight	Accepted for mission flexibility
Retractable landing gear	Lower cruise drag and better range	More complexity and weight	Selected over fixed gear

High-altitude cruise	Lower drag and better range	Reduced available engine power	9 km cruise selected
High-throttle cruise	Faster medevac response	Much higher fuel burn	Used only for time-critical missions

The most important tradeoff was wing sizing. A large wing was necessary to meet the 500 ft takeoff and landing requirement, especially with Fowler flaps. The penalty is increased drag and structural weight, but the STOL requirement made this tradeoff necessary.

The propulsion trade was also critical. The PT6A-60A engines provide much more climb performance than required, giving Borealis a strong safety margin. The downside is increased fuel burn at high throttle, so normal missions should use efficient cruise settings rather than maximum power.

The fuselage tradeoff favored mission usefulness over minimum drag. A smaller fuselage would improve cruise efficiency, but it would reduce cargo and medevac capability. Since Borealis is meant to serve remote Arctic communities, internal flexibility was prioritized.

Overall, the selected design is a balanced solution. Borealis is not optimized for one single metric; it is optimized to meet the full mission: short-field operation, Arctic reliability, flexible payload use, safe climb performance, and acceptable cruise efficiency.

Chapter 5
Conclusion

Process, Results and Importance

The Borealis design process required balancing several competing requirements: short-field performance, Arctic reliability and redundancy, cruise efficiency, payload flexibility, and minimized operating cost. The final aircraft configuration reflects this balance through a high-wing, twin-turboprop layout with a cruciform tail, retractable tricycle landing gear, and a modular cabin capable of supporting passenger, cargo, and medevac missions. Each major design decision was driven by the operational needs of remote Arctic service, where aircraft must operate safely from short gravel runways, withstand extreme cold, and remain useful across multiple mission types.

The final design satisfies the primary performance requirements established for the project. Borealis meets the 500 ft takeoff and landing constraint over a 50 ft obstacle through a large wing, high-lift Fowler flaps, low stall speed, and strong turboprop thrust. The selected PT6A-60A engines provide a climb rate well above the required 800 ft/min at maximum takeoff weight, giving the aircraft a significant safety margin during obstacle clearance and departure from remote runways. Cruise and mission simulations also show that Borealis can complete the required 450 nmi reference mission while maintaining the required average speed and preserving fuel reserves. Although range remains one of the most sensitive design constraints, the aircraft still satisfies the mission requirement with positive remaining fuel.

The design also demonstrates the importance of system-level tradeoffs in aircraft sizing. Increasing wing area improved STOL capability but increased wetted area, structural weight, and parasite drag. The large fuselage allowed practical passenger, cargo, and medevac layouts but also increased empty weight and drag. The twin-engine propulsion system increased acquisition and operating cost compared with single-engine aircraft, but it provided the redundancy and climb performance needed for Arctic operations. These tradeoffs show that Borealis was not optimized around one isolated metric, but around the complete mission environment.

Overall, Borealis represents a practical and capable Arctic utility aircraft concept. It combines proven configuration choices with mission-specific sizing to produce an aircraft suited for remote transportation, emergency medical response, and cargo support. Its strongest advantages are short-field capability, twin-engine safety, FIKI readiness, gravel runway compatibility, and rapid cabin reconfiguration. While further refinement would be required in detailed structural design, certification analysis, and cost modeling, the preliminary results show that Borealis is a feasible and competitive solution for modern Arctic aviation needs.

Chapter 6

Bibliography

[1] Raymer, D. P., *AIAA Fundamentals of Aircraft Design*, Appendix I.

[2] Raymer, D. P., *AIAA Fundamentals of Aircraft Design*, Chapter 5.

[3] Raymer, D. P., *AIAA Fundamentals of Aircraft Design*, Chapter 20.

[4] Anderson, J. D., *Fundamentals of Aerodynamics*.

[5] Federal Aviation Administration, "14 CFR § 91.527 — Operating in icing conditions," Legal Information Institute, Cornell Law School. Available: https://www.law.cornell.edu/cfr/text/14/91.527.

[6] Absolute Generators, "AGi7P Specifications Sheet." Available: https://www.absolutegenerators.com/media/blfa_files/AGi7P-_Specifications_Sheet.pdf.

[7] Wikipedia, "Aerial firefighting." Available: https://en.wikipedia.org/wiki/Aerial_firefighting.

[8] Wikipedia, "Lockheed L-188 Electra." Available: https://en.wikipedia.org/wiki/Lockheed_L-188_Electra.

[9] Wikipedia, "DC-10 Air Tanker." Available: https://en.wikipedia.org/wiki/DC-10_Air_Tanker.

[10] Wikipedia, "Canadair CL-415." Available: https://en.wikipedia.org/wiki/Canadair_CL-415.

[11] Avincis, "CL-415 Specifications Flyer." Available: https://www.avincis.com/wp-content/uploads/2024/11/A4-CL-415-Specifications-Flyer-Low-Res.pdf.

[12] Wikipedia, "Pratt & Whitney Canada PW100." Available: https://en.wikipedia.org/wiki/Pratt_%26_Whitney_Canada_PW100.

[13] SKYbrary, "CL2T — Canadair CL-415." Available: https://skybrary.aero/aircraft/cl2t.

[14] Wikipedia, "De Havilland Canada DHC-6 Twin Otter." Available: https://en.wikipedia.org/wiki/De_Havilland_Canada_DHC-6_Twin_Otter.

[15] "AME 261 Handouts" *Appendix A: Drag Build Up for the Fuselage and other Components.*

[16] "Aircraft Specs." Dynamic Aviation, Available:
dynamicaviation.com/aircraft-specs

^ *Note, used for comparisons with other aircraft, and for engine information*

[17] Meyer, Austin. *"PT-6 Operation."* Austin Meyer, Available:
https://austinmeyer.com/pt-6-operation/.

^ *Note, used for more PT6A engine family information, such as specific fuel consumption*

[18] Wikipedia, *"Pratt & Whitney Canada PT6."* Available:
https://en.wikipedia.org/wiki/Pratt_%26_Whitney_Canada_PT6.